

United States
Environmental Protection
Agency

Environmental Sciences Research
Laboratory
Research Triangle Park NC 27711

600/4-79-051
May 1979

Research and Development



The EPA Meteorological Wind Tunnel

Its Design,
Construction, and
Operating
Characteristics



RESEARCH REPORTING SERIES

Research reports of the Office of Research and Development, U.S. Environmental Protection Agency, have been grouped into nine series. These nine broad categories were established to facilitate further development and application of environmental technology. Elimination of traditional grouping was consciously planned to foster technology transfer and a maximum interface in related fields. The nine series are:

- 1 Environmental Health Effects Research
- 2 Environmental Protection Technology
- 3 Ecological Research
- 4 Environmental Monitoring
- 5 Socioeconomic Environmental Studies
- 6 Scientific and Technical Assessment Reports (STAR)
- 7 Interagency Energy-Environment Research and Development
- 8 "Special" Reports
- 9 Miscellaneous Reports

This report has been assigned to the ENVIRONMENTAL MONITORING series. This series describes research conducted to develop new or improved methods and instrumentation for the identification and quantification of environmental pollutants at the lowest conceivably significant concentrations. It also includes studies to determine the ambient concentrations of pollutants in the environment and/or the variance of pollutants as a function of time or meteorological factors.

EPA-600/4-79-051
September 1979

THE EPA METEOROLOGICAL WIND TUNNEL
Its Design, Construction and Operating Characteristics

by

William H. Snyder
Meteorology and Assessment Division
Environmental Sciences Research Laboratory
U.S. Environmental Protection Agency
Research Triangle Park, NC 27711

ENVIRONMENTAL SCIENCES RESEARCH LABORATORY
OFFICE OF RESEARCH AND DEVELOPMENT
U.S. ENVIRONMENTAL PROTECTION AGENCY
RESEARCH TRIANGLE PARK, NC 27711

DISCLAIMER

This report has been reviewed by the Environmental Sciences Research Laboratory, U.S. Environmental Protection Agency, and approved for publication. Mention of trade names or commercial products does not constitute endorsement or recommendation for use.

AFFILIATION

William H. Snyder is a physical scientist in the Meteorology and Assessment Division, Environmental Sciences Research Laboratory, U.S. Environmental Protection Agency, Research Triangle Park, North Carolina. He is on assignment from the National Oceanic and Atmospheric Administration, U.S. Department of Commerce.

PREFACE

The EPA Meteorological Wind Tunnel (MWT) is described in detail in this report. The basic aerodynamic design and specifications were provided by EPA personnel. The tunnel is quite similar in overall size, shape and performance characteristics to the Environmental Wind Tunnel (EWT) at Colorado State University (CSU). Plans for the EWT were purchased from CSU and many ideas were incorporated into the EPA MWT. It was constructed by Aerolab Supply Company of Laurel, Maryland. Professor A. W. Sherwood, President, Aerolab Supply, provided numerous innovations that improved its performance and simplified its construction. The tunnel was commissioned in June, 1974.

The impetus for this report came primarily from a statement by Bradshaw and Pankhurst (1964) that tunnel designers should "calibrate their tunnels properly and publish the results, good or bad, so that wind tunnel design may come to involve more science, less art, and no magic at all." It will also, of course, serve numerous other purposes.

ABSTRACT

The design philosophy, construction details, and operating characteristics of the EPA Meteorological Wind Tunnel are described. Measurements in the empty tunnel show that the mean velocity is uniform to within $\pm 2\%$ at any given cross section, at speeds as low as 1.5 m/s. The turbulence intensity in the empty tunnel is typically 0.5%. A 2-meter-deep boundary layer was obtained using elliptic wedge vortex generators and roughness on the floor. Measurements are presented showing that this boundary layer simulates, in both turbulence structure and dispersive characteristics, a neutral atmospheric boundary layer over rural terrain.

CONTENTS

PREFACE	iii
ABSTRACT.	iv
FIGURES	vi
ACKNOWLEDGEMENTS.	viii
1. INTRODUCTION.	1
2. CONCLUSIONS	5
3. DESIGN AND CONSTRUCTION DETAILS	6
3.1 Design Philosophy.	6
3.2 Gross Characteristics.	8
3.3 Entrance Section	8
3.4 Test Section	9
3.5 Acoustic Silencers	12
3.6 Power Section.	12
3.7 Tail Section Assembly.	13
3.8 Instrument Carriage.	14
3.9 Operator's Console	15
4. THE LABORATORY AND INSTRUMENTATION.	16
4.1 The Laboratory	16
4.2 The Minicomputer	16
4.3 Flow Measurement Apparatus	17
4.4 Concentration Measurement Apparatus.	18
5. PERFORMANCE CHARACTERISTICS OF THE WIND TUNNEL.	19
5.1 Calibration of Empty Tunnel.	19
5.2 Development of Two-Meter-Thick Boundary Layer.	21
REFERENCES.	27

FIGURES

<u>Number</u>		<u>Page</u>
1	Overview of the EPA Meteorological Wind Tunnel.	28
2	Overall plan and elevation of the EPA Meteorological Wind Tunnel	29
3	Front, side, and top views of entrance section.	30
4	Perspective and side views of entrance section.	31
5	Test section details.	32
6	Inside view of test section looking downstream.	33
7	Turntable and details	34
8	Turntable mounted on dolly.	35
9	Turntable dolly	36
10	Details of adjustable ceiling support	37
11	Overview of adjustable ceiling support.	38
12	Gear motor, limit switches, and torque tube	39
13	Inlet silencer.	40
14	Exhaust silencer.	41
15	View of fan and motor from inside sound enclosure	42
16	Tail section assembly	43
17	Instrument carriage	44
18	Views of instrument carriage.	45
19	Close-up view of cable drum	46
20	Operator's console.	47
21	Floor plan of Fluid Modeling Facility	48
22	Schematic of minicomputer system.	49
23	Typical calibration curve for hot-film probe.	50
24	Effect of trip ring on velocity and velocity fluctuations	51
25	Calibration of empty wind tunnel: air speed as a function of fan speed	52

<u>Number</u>		<u>Page</u>
26	Lateral profiles of mean velocity and turbulence intensity; $U = 1.5$ m/s	53
27	Vertical profiles of mean velocity and turbulence intensity; $U = 1.5$ m/s	54
28	Vertical profiles of mean velocity and turbulence intensity; $U = 3$ m/s	55
29	Vertical profiles of mean velocity and turbulence intensity; $U = 6$ m/s	56
30	Vortex generator system.	57
31	Development of mean velocity profile along centerline of wind tunnel; $U = 3$ m/s (except as noted).	58
32	Mean velocity profiles in log-law form	59
33	Development of longitudinal turbulence intensity along centerline of wind tunnel; $U = 3$ m/s (except as noted).	60
34	Development of vertical turbulence intensity along centerline of wind tunnel; $U = 3$ m/s (except as noted).	61
35	Development of Reynolds stress along centerline of wind tunnel; $U = 3$ m/s (except as noted)	62
36	Lateral uniformity of mean velocity; $U = 3$ m/s	63
37	Lateral uniformity of longitudinal turbulence intensity; $U = 3$ m/s	64
38	Lateral uniformity of vertical turbulence intensity; $U = 3$ m/s	65
39	Lateral uniformity of Reynolds stress; $U = 3$ m/s	66
40	Lateral concentration profiles taken through plume centerline; $U = 3$ m/s.	67
41	Vertical concentration profiles taken through plume centerline; $U = 3$ m/s.	68
42	Estimated wind-tunnel dispersion parameters compared with standard Pasquill-Gifford values (Turner, 1970)	69

ACKNOWLEDGEMENTS

The number of people who helped in establishing the Fluid Modeling Facility is too large to mention individually. Special mention and thanks, however, must be extended to Mr. Robert A. McCormick, who cleared the path for the EPA Fluid Modeling Facility; Mr. Roger Thompson, who aided in the aerodynamic design of the wind tunnel; Professor J.E. Cermak, who provided several ideas and helpful suggestions for improving the tunnel; Mrs. Cooper Atamanchuk, for her flexible and common-sense contracting abilities; Mr. A. Wiley Sherwood, who with his engineering genius and pragmatic views, constructed a functional and economical wind tunnel with high quality flow characteristics; and Mr. Robert E. Lawson, Jr. for his enduring and painstaking efforts to keep the laboratory running smoothly.

1. INTRODUCTION

Under the Clean Air Act of 1967 (amended in 1970 and 1977), the U.S. Environmental Protection Agency (EPA) is charged with the responsibility of overseeing and enforcing air pollution control measures. Essential ingredients of this responsibility are the identification of air pollutants and the determination of their concentrations in the atmospheric boundary layer. One of the primary responsibilities of the Meteorology and Assessment Division (MD) is to develop and evaluate models to predict the transport and diffusion of pollutants from source to receptor. Other responsibilities of the MD include the evaluation of Environmental Impact Statements and the provision of support to other federal agencies, Regional Offices of the EPA, and state and local air pollution control agencies. To date, this support has been provided primarily through the development and application of mathematical models. To develop the models, EPA has relied almost exclusively on field programs.

In spite of the tremendous advances in computer sizes and numerical techniques, mathematical models still require gross simplifications, both because the fundamental fluid-dynamical processes involved in the dispersion of materials are not well-understood and because computer memories are still far too small to keep track of the detailed eddy motions in the atmospheric boundary layer.

Field programs to obtain experimental data are extremely expensive and time consuming. Data are required for various combinations of meteorological conditions, various kinds of terrain, different source heights, various types of sources, etc. Present mathematical models are suitable only where adequate diffusion data exist or can be inferred, that is only for continuous point sources fairly close to the ground over relatively flat terrain. They are not suitable for calculating concentrations of contaminants in building wakes, in hill-valley complexes, from high sources, within the domain of the urban heat island, etc.

In the past two decades, fluid (laboratory) models have shown great potential for solving many of the complex fluid-dynamical problems that are presently intractable through analytical/numerical techniques. Fluid models appear to work best where mathematical models fail (i.e., where obstructions such as buildings and hills block the flow). They show great promise for simulating the urban heat island circulation, mountain-valley winds and even transient phenomena such as the inversion break-up. In a few weeks in the laboratory where atmospheric conditions may be controlled at will, answers may be had that would require years of expensive field measurements.

A study was conducted to determine the feasibility of fluid modeling and the usefulness of such a facility to the EPA (Snyder, 1972a). The final report on that study included a critical review of the similarity criteria necessary to model atmospheric motions (Snyder, 1972b), an extensive review of the pertinent literature, descriptions of the facilities of the major modeling establishments throughout the world (Snyder, 1974), and recommendations concerning actions to be taken by EPA along the lines of fluid modeling of air pollution meteorology. The conclusion of that study was a recommendation that a complete fluid modeling facility be established that would include: (1) an open-return, nonstratified wind tunnel (designed such that stratification capabilities could be added at a later date), (2) a water channel/towing tank with provisions for salt-water stratification, and (3) a complete laboratory, including shops and staff.

The objectives of the fluid modeling program are, in order of priority:

- (1) To establish the areas of applicability of fluid modeling and to delineate the similarity criteria, i.e., to set the standards for fluid modeling of atmospheric diffusion,
- (2) To conduct basic, systematic studies of the flow and diffusion of pollutants in the atmospheric boundary layer, in particular, in complex flow situations (around hills, buildings and highways), to aid in the construction and development of mathematical models, and to aid in the understanding of such flows, and
- (3) To conduct applied model studies, thereby providing direct support to other federal agencies and to EPA Regional offices.

The first objective, setting the standards, is given top priority. Neither proper rules nor areas of applicability of fluid modeling are well-established. Various laboratories apply different, often conflicting,

similarity criteria to essentially the same modeling problems. Frequently, reports of these studies are included as portions of Environmental Impact Statements prepared by industry. Setting the standards is essential if EPA is to: (1) make rational decisions on the Environmental Impact Statements, and (2) conduct modeling studies of its own. EPA's role should be to determine what types of problems can be solved through fluid models, what similarity criteria need to be applied in particular cases, how much detail is required in the models, etc. An essential part of this objective is the critical comparison of model results with full scale field data.

Basic, systematic studies are given higher priority than applied (specific) studies. Applied problems are useful, but in general, do not enhance the understanding of the basic fluid mechanics. They do not enable one to predict the effects of slight modifications to the model or to the flow. Historically, this has been a major objection to wind tunnel studies. As an example, many, many wind tunnel studies have been concerned with the problem of downwash of effluents in the vicinity of industrial plants. The sponsors have been, in almost all cases, the industries that are building or modifying their own plants, and they have not been interested in broadening the scope of the study so that the results could be generalized and made universally applicable. Thus, in spite of up to 40 years of wind tunnel modeling of industrial plant downwash, we still cannot predict with any certainty what the ground level concentrations will be for a new plant without running yet another wind tunnel study. EPA's role here should be to conduct basic, general and systematic studies so that, for the above example, a "building codes" handbook could be compiled.

The first step in the establishment of the Fluid Modeling Facility was the acquisition of the Meteorological Wind Tunnel, which is described in detail in this report. Brief descriptions of the laboratory and equipment are also given. The second major step is the acquisition of the Water Channel/Towing Tank, which will be described in a separate report. The third major step in the over-all plan is the closing of the return of the wind tunnel and the addition of floor heating and cooling to provide for temperature stratification of the flow. Because of the very large expense and the "down-time" involved in this third step, its execution has been postponed indefinitely.

In Section 3, the design and construction details of the wind tunnel will be discussed. Brief descriptions of the laboratory and its equipment are given in Section 4. Calibration data on the performance of the empty wind tunnel as well as measurements of the structure and dispersive characteristics of a 2-meter thick simulated atmospheric boundary layer are presented in Section 5.

2. CONCLUSIONS

A meteorological wind tunnel has been constructed for the purpose of studying the pollutant transport and dispersion characteristics of complex flows such as those around hills and buildings. It is a very low speed, open return tunnel with a long test section (2.1 x 3.7 x 18.3 m) that will accomodate model sizes from individual buildings at a scale ratio of 1:300 to large terrain at 1:5000. Design and construction features of the tunnel as well as the laboratory and instrumentation used for measurements in the tunnels are described in detail.

The empty wind tunnel was calibrated and its performance characteristics are described. A "surging" problem was discovered and corrected. Mean velocities were found to be uniform to within $\pm 2\%$ at any cross section, and the turbulence intensity was found to be typically 0.5%. Both these characteristics apply even at speeds as low as 1.5m/s and may be regarded as excellent performance characteristics.

A 2-meter thick boundary layer was developed in the tunnel using a vortex generator system to simulate the atmospheric boundary layer. The properties of this boundary layer are reported in detail. It is a slowly developing boundary layer that simulates the neutral atmospheric boundary layer over rural terrain. It is reasonably two-dimensional and its dispersive characteristics match "accepted" atmospheric data. This boundary layer would be suitable for comparative types of studies dealing with flow and diffusion patterns in the near-field of individual buildings, but further testing would be required to determine its suitability for longer range studies.

3. DESIGN AND CONSTRUCTION DETAILS

3.1 Design Philosophy

A meteorological wind tunnel differs in two basic respects from a conventional aeronautical wind tunnel. First, because the atmospheric boundary layer usually extends far above the buildings immersed in it, the simulated boundary layer in the meteorological wind tunnel must be quite deep in order for the model buildings to be of reasonable size. In an aeronautical wind tunnel, the reverse is required - great pains are taken to minimize the thickness of the boundary layers, to make the flow uniform across the test section, and to obtain as low a turbulence intensity as is feasible. A very long test section is generally required in a meteorological wind tunnel in order to generate a thick boundary layer. Second, high wind speeds are generated in aeronautical wind tunnels to compensate for the reduced size of the models. However, because buoyancy effects are much more important in atmospheric flows, wind speeds in meteorological wind tunnels are generally reduced in order to accommodate these buoyancy effects. In aeronautical terminology, then, the EPA tunnel would be classified as an "ultra-low speed" tunnel. Because low turbulence is not a primary goal in the meteorological wind tunnel, a large contraction ratio is not essential. Also, because of the low speed, power consumption is minimal and the capital cost of closing the return is not justified by the savings in operating costs. Thus, the EPA Meteorological Wind Tunnel (MWT) was designed to be an ultra-low speed, open-return type with a relatively small contraction ratio (3:1) and an unusually long test section (18 m).

The overall size of the MWT was determined by the size of the test section, which, in turn, was determined by the types of models to be used. (Many factors, of course, enter into the decision on the size of the tunnel, but only the primary ones are discussed here.) The spectrum of model types to be studied in the tunnel ranged from individual buildings at a scale ratio of, say, 1:300, to topographical models at scale ratios of up to 1:5000. If

the atmospheric boundary layer is taken to be 600 m in depth, then the test section height must be somewhat larger than 2 m in order to accommodate a simulated atmospheric boundary layer for building studies. A 2.1 m test section height was chosen for convenience, both to reduce blockage effects of large models and to accommodate model scale ratios as large as 1:300. At a scale ratio of 1:500, the model height of a modern power plant would be about 30 cm, and the model stack height would be about 60 cm. Allowing for modeling some of the surrounding buildings and terrain irregularities, and also for side wall boundary layers, the width of the test section was chosen to be 3.7 m. Indications were that confidence could not be placed in model predictions for downwind distances much larger than about 5 kilometers (Snyder, 1972b). The required length of test section was thus 18.3 meters: approximately 10 m for the downwind distance, 3 m for the model and upwind terrain, and 5 m for boundary layer generators and development of the appropriate boundary layer structure.

The design maximum speed was set at 8 m/s. Higher speeds are seldom required; this is a matter of considerable economic importance, since power consumption varies with the cube of the speed. The tunnel was designed to be controllable over as wide a speed range as possible to allow for possible future modifications. To permit modeling of buoyant plumes, the tunnel was to be capable of operating at very low speeds as well (say, 30 cm/s). The size and speed of the tunnel are comparable with other recently constructed wind tunnels for the study of atmospheric diffusion and meet the design criteria put forth by Sundaram and Ludwig (1970).

Convenience of operation was a major factor influencing the design of the tunnel. To this end, the test section was divided into five identical subsections with interchangeable windows and floor sections. Transparent windows are interchangeable with opaque (flat black) panels, thereby providing the option of good visibility of the interior of the tunnel or an opaque background for photography. One of the floor sections contains a removable turntable, and because of the interchangeability of the floor sections, the turntable may easily be placed in any of the five subsections. The turntable rests on a four-wheeled dolly with an elevating mechanism; it can easily be rotated to change the wind direction over the model or it can be lowered from the tunnel and rolled to the shop; a different model

mounted on a second turntable may be installed in the tunnel in a matter of minutes. An instrument carriage is included to provide for three-dimensional positioning of measuring probes with remote control and readout of position. All controls and readout devices are centrally located on an operator's console.

3.2 Gross Characteristics

Figure 1 shows an overview of the EPA Meteorological Wind Tunnel and Figure 2 provides a sketch showing the major dimensions and labeling the various sections. The overall length of the tunnel is 38.2 m and its maximum height and width are 4.62 m and 6.43 m, respectively. Room air enters the tunnel at the left through a honeycomb and a series of four screens that remove the disturbances from the room air and produce a uniform velocity profile. The flow then passes through a contraction that further reduces the turbulence and also aids in producing a uniform velocity profile. The flow then passes through the test section, an acoustic silencer, a rectangular to round transition section, the fan, a diffuser, and finally another acoustic silencer from which it exhausts back into the room. The fan section is totally enclosed in a sound attenuating enclosure. The ceiling height in the test section is adjustable to obtain a zero pressure gradient and to compensate for blockage effects of the model.

3.3 Entrance Section

Details of the entrance section are shown in Figures 3 and 4. The bellmouth is formed using a 15 cm diameter pipe, tangent to the inside surface of the tunnel, around the entire perimeter of the entrance. The entrance dimensions are 4.0 m x 5.5 m. The floor of the entrance section is 48 cm from the building floor.

The flow straightener consists of a VerticelTM plastic impregnated paper honeycomb with triangular shaped cells, cell "diameter" of 1.27 cm and cell length of 15 cm. The cell length-to-diameter ratio of 12, substantially larger than the ratio of 6 to 8 recommended by Bradshaw and Pankhurst (1964), was felt to be necessary at these especially low entrance velocities for removing swirl and lateral mean velocity variations caused by disturbances to the room air from draughts and obstructions.

Four stainless steel anti-turbulence screens of mesh size 7.9/cm (20/in) and wire diameter 0.025 cm (0.010 inch) were specially woven by

Tyler Manufacturing, Cleveland, OH, to cover the entire inlet area without seams. This type of screen provides an open area ratio (β) of 64% and a local Reynolds number ($U_\infty d / \nu$) of 80. These parameters yield a pressure drop coefficient of 0.71 (Davis, 1957), which theoretically provides a reduction factor for mean velocity variations of 0.48 and a turbulence intensity reduction factor of 0.76, for each screen (Pankhurst and Holder, 1952). For four screens the respective factors are 0.05 and 0.34. The screens are spaced 20 cm (800 wire diameters) apart. This spacing is sufficient for the turbulence generated in the wire wakes of one screen to decay before the next screen is reached. It is also sufficient for insertion of a long-handled vacuum wand for cleaning.

The screens are fastened to vertical aluminum pipes outside the two sides; the pipes may be rotated to tension the screens. Downstream of the last screen a settling section about 1 m long allows the turbulence in the wakes of the screen wires to decay.

With an entrance area of 4.0 m x 5.5 m and a test section area of 2.1 m x 3.7 m, the contraction ratio is 2.8:1. The length of the contraction is 3.3 m. The profile shape approximates two cubic arcs joined together with equal slopes to form a smooth transition at the inflection point, which is located approximately 1.2 m downstream from the entrance to the contraction. The actual shape represents a compromise based on several theoretical papers and previous designs and experiences of Aerolab Supply Co., Laurel, MD (A. W. Sherwood, private communication). Table 1 lists the dimensions of the contraction.

3.4 Test Section

Details of the test section are shown in Figure 5. A view of the interior is provided in Figure 6. The inside height, width and length are 2.1, 3.7, and 18.3 m, respectively. The sections are fabricated with 6.4 x 6.4 cm (2 1/2 x 2 1/2 in) angle iron frames that retain 1.9 cm (3/4 in) plywood and 1.27 cm (1/2 in) acrylic plastic (plexiglasTM) panels. One of the floor panels is fitted with a 3.2 m diameter turntable that can be manually rotated to any desired yaw angle with the air stream. Since all the floor panels are of the same outside dimensions, the panel containing the turntable can be placed in any of the five subsections. This involves the exchange of a solid section for the turntable section through the use of a specially constructed

TABLE 1. CONTRACTION DIMENSIONS

Distance from Entrance (cm)	Inside Width (cm)	Inside Height (cm)
0	549	396
30	540	392
61	529	380
91	505	355
122	477	324
152	449	298
183	424	275
213	403	255
244	387	236
274	374	224
305	368	215
335	366	213

lifter. It consists of casters fitted on the ends of lengths of square tubing which are bolted to the floor panels at the two sides through threaded metal inserts in the plywood floor. The floor panel to be moved is attached to the lifter and rolled along tracks (floor supports at the sides of the test section) to its new position. All floor panels are sealed at the edges by strips of foam rubber to minimize air leakage into the tunnel. To facilitate ease in movement of the floor panels, they were made as light and thin as possible. To prevent sagging, adjustable jacks support the centers of the floor panels.

Two circular turntables (Figures 6 and 7) are included so that one can be fitted with models while the other is under test in the tunnel. A four-wheeled dolly with an elevating mechanism (Figures 8 and 9) transports the turntable from the shop to the tunnel, lifts the turntable to its position in the tunnel, and allows rotation of the model in the tunnel. Two dollies are provided: One is a hand-crank version; the other is motorized. The joint between the turntable and tunnel floor is sealed with a gasket and toggle clamps as shown in Figure 7.

The sidewalls are 2.44 m in height, the entire lower halves of which are fitted with acrylic plastic windows in three of the five subsections. The other two subsections contain opaque (plywood) windows that are interchangeable with the transparent ones for photographic purposes. Since the windows are heavy, a trolley system running on rails at the top of each side is provided to facilitate handling. A fluorescent light fixture is attached to the top of each transparent window to provide light inside the tunnel. Convenience outlets and switches are provided at each section for the lights and miscellaneous equipment. The windows are sealed at the seams with foam rubber that is compressed by the action of the toggle clamps retaining the windows. Covered, 2.5 cm portholes provide access for electrical cables inside the tunnel.

The ceiling (see Figure 5) is fabricated of 0.95 cm (3/8 in) marine plywood to provide greater flexibility as compared to the 1.9 cm (3/4 in) floor and sidewall panels. The individual plywood sheets are edge-glued and laterally stiffened at 61 cm intervals with cross battens of 2.54 cm (1 inch) square steel tubing. The ceiling is supported at 112 points by whiffle trees attached to roller chain (see Figures 10 and 11). The chain is carried by sprockets rotated by 14 torque tubes oriented transversely across the top of the tunnel at 1.2 m intervals. Separate gearmotor drives (Dayton Model 6K303, 30 RPM, 1/20 KW, 115 V, Ratio 57.5:1) with speed reducers (Dayton Model 2Z421AWK, Ratio 60:1) on each of the torque tubes enable an operator to put a smooth contour in the ceiling. Limit switches prevent the movement of the ceiling more than 30 cm in either direction. Switches at the operator's console control the gearmotors. A pointer attached to a bracket near each torque tube provides a measurement of the ceiling height to a person at the operator's console. Electromagnetic disc brakes (Dayton Model 3M342, 115V, 60 Hz, 0.1 kg-m torque) on the gear motors prevent the torque tubes from rotating when the power is turned off. Figure 12 presents a close-up view of the ceiling lift mechanism. A hinged (sliding) flap over the inlet silencer at the downstream end of the test section connects the flexible ceiling to the transition section. Windows (57 x 122 cm) spaced every 1.2 m in the ceiling provide for overhead lighting and photographing of models from above. Clothesline retractors take up the slack on the roller chains. A catwalk to facilitate personnel access to the top of the tunnel has been added since

the photograph in Figure 11 was taken.

The edges of the ceiling are sealed within the sidewalls by strips of linear polyethylene that are guided by aluminum strips at the edges of the ceiling (Figure 10). An inflatable gum rubber tubing (amber surgical) forces the plastic sealing strips against the tunnel sidewalls when air pressure is applied within the tubing. The tubing is deflated to adjust the ceiling height and inflated to 70 to 100 kPa (10 to 15 psi) to make the seal after the appropriate height is obtained.

3.5 Acoustic Silencers

The mechanical and aerodynamic noise emanating from the fan is reduced by acoustic silencers. The inlet and outlet sections of the fan are fitted with interior partitions forming a large honeycomb of plywood. All surfaces of the cells thus formed are covered with a 2.5 cm thick sound-absorbent material (Lina-Coustic fiberglass duct liner) that is cemented to the plywood and protected at the leading and trailing edges with formed and perforated sheet steel. The inlet silencer is 2.1 m x 2.7 m in cross section, 2.4 m in length, and is divided into 12 cells. A photograph of the inlet silencer is shown in Figure 13. The outlet silencer, shown in Figure 14, is of similar construction. It is 3 m square, 2.4 m in length, and consists of 12 cells. The exterior of the fan section, from inlet silencer to outlet silencer, is completely housed by a double-walled enclosure of gypsum sound deadening board. The interior and exterior wall coverings are independently supported by separate frameworks. A fiberglass blanket is placed in the space separating the walls. The enclosure contains a door for access to the power section and two windows to provide cooling air to the motor and eddy-current coupler. The noise level in the room when the tunnel is run at maximum speed is approximately 60dba.

3.6 Power Section

The fan is a 1.8 m (6 ft) diameter axial flow fan with 5 adjustable pitch blades manufactured by Buffalo Forge Company (Size 72D5, design II, type S, Adjustax Vaneaxial, Arr. 9). It is driven through a V-belt drive by an Eaton Dynamic Eddy Current Coupling (Model No. ACM 9143, 75 KW, Max. Speed 1685 RPM) to provide variable rotational speed. The coupling is driven by a constant speed AC motor (Westinghouse, 75 KW, 1770 RPM, 3 ph, 60 Hz, 230/460 V) with a reduced voltage starter. This power system is very easy to

operate, provides a quite steady air flow rate and a wide range of speed, and produces a minimum of noise. To start the tunnel, the operator need only push the motor start button, then the coupling start button, then turn the speed adjustment knob to obtain the desired tunnel speed (the one-turn potentiometer supplied by the manufacturer was replaced by a ten-turn meter for finer resolution of speed setting). The fan rotational speed is continuously monitored using a photomechanical light chopper (40 hole disc mounted on the fan shaft and an electronic counter). The maximum fan speed is 900 RPM (~ 8 m/s). It is quite steady as low as 20 RPM (~ 0.15 m/s). This type of system was chosen over a variable pitch fan with a two-speed motor for two reasons: (1) a variable pitch fan generally functions efficiently for the high tunnel speeds, but at low air speeds the pitch must be reduced to the point where the blade sections near the hub produce an axial velocity distribution affecting the flow in the tunnel. The use of a two-speed motor on a variable pitch fan tends to alleviate this condition, but it remains a serious defect. (2) also, because the noise generated by a variable pitch fan is primarily a function of the blade tip speed, the noise level is essentially the same (high) at all tunnel speeds. Figure 15 shows a view of the fan and drive motor from inside the sound enclosure.

3.7 Tail Section Assembly

Details of the tail section assembly are shown in Figure 16. A 2.4 m (8 ft) long transition section of 0.48 cm (3/16 in) thick steel was developed by triangulation to connect the rectangular acoustic silencer to the round fan. A safety screen was placed at the entrance to the transition section to prevent debris from entering the fan. A flexible rubber joint connects the transition section to the fan to prevent vibrations of the fan from being transmitted to the remainder of the tunnel. A 3.7 m long round diffuser with inlet diameter of 1.83 m and a divergence angle of 13.5° (total angle) saves energy by converting some kinetic energy into pressure energy. This rather large divergence angle is considerably larger than that (5°) recommended by Pankhurst and Holder (1952), but, because of the low energy consumption, an efficiency approaching 80% was felt to be adequate when compared with the resulting savings in capital costs and floor space from a shorter diffuser. However, as will be explained later, this large divergence angle created problems of surging. The problem was eventually alleviated by installing a

trip ring as suggested by Pope and Harper (1966). The trip ring was a 2.54 cm wide piece of thin metal installed circumferentially around the entrance to the diffuser. The resulting loss in top speed of the tunnel was insignificant (less than 5%).

The fan, diffuser, motor and coupler are bolted rigidly to a framework that is supported by coil springs to permit some movement (see Figure 16). The downstream end of the diffuser is connected to another transition section through a second flexible rubber joint. The second transition is 1.83 m long and has an octagonal entrance and a square exit. The flow exiting the diffuser thus sees an abrupt shape change from round to octagonal.

3.8 Instrument Carriage

Figures 17 and 18 show the details of the instrument carriage which provides the capability of positioning a probe anywhere within a 17 m x 3 m x 1.5 m parallelepiped to an accuracy of ± 1 mm. The positioning, control, and readout are effected remotely from the operator's console. The slewing rate in all three coordinate directions is adjustable to provide fast positioning for long traverses and slow rates for accurate settings in the vicinity of the set point.

The main support frame is a 5.1 x 15.2 cm (2 x 6 in) tubular steel member. Longitudinal positioning (x-direction) is provided by a gearmotor (Dayton Model 3M234, 1/20 KW, 2.8 RPM) driving a sprocket-chain arrangement, which in turn drives wheels that roll on tracks on each side of the test section. The tracks are 5 x 10 cm (2 x 4 in) tubular steel running the length of the test section 1.4 m above the floor. They are slotted to house power and signal cables inside. A pneumatic cylinder (Schraeder Model 3452A) actuates a two-speed transmission that provides high and low speed ranges. Maximum speeds are 5000 and 700 mm/min on the high and low ranges respectively.

A block driven by a roller chain on a vertical bar provides for vertical positioning (z-direction) of the probe. The bar is fastened to a yoke that slides transversely on the mainframe. Vertical drive is effected through a gearmotor (Dayton Model 3M234, 1/20 KW, 2.8 RPM) that drives a square shaft (parallel to the mainframe), that, in turn, drives a mating sprocket fastened to the vertical bar. The sprocket slides axially on the square shaft. Maximum speed in the vertical direction is 400 mm/min.

Transverse positioning (y-direction) is provided by a gearmotor (Dayton Model 3M235, 1/20 KW, 6.7 RPM) that slides the yoke on the mainframe via a looped roller chain. Maximum speed in the transverse direction is 1000 mm/min.

Theta Instruments, Inc. optical encoders (Model Nos. 05-100-31-2 and 05-250-31-2) sense the probe motion through drive mechanisms similar to those of the gearmotors, except that special care has been taken to minimize backlash. The gearmotors are mounted on one side of the mainframe, with power cables run through the slotted track on the test section sidewall. The optical encoders are mounted on the opposite side of the mainframe, with signal cables run through the other slotted track on the test section sidewall, in order to minimize electrical noise and interference from the gearmotors and power cables. The cables are wound on large drums at the downstream end of the test section (See Figure 19). Hanging weights on the drums provide constant tension on the cables to take up slack when the carriage is moved downstream. The cables then wind and unwind from smaller drums on the outside of the tunnel, from which they are routed to the operator's console. Blockage of the cross-sectional area by the carriage is approximately 3.5%.

On/off reversing switches and silicon-controlled rectifiers at the operator's console provide power to the gearmotors. Monsanto electronic reversible counters (Model 106A) provide direct readout in millimeters of the x, y, and z coordinate positions of the probe. The coordinates can be "zeroed" at any position to establish an origin.

3.9 Operator's Console

The operator's console is shown in Figure 20. All tunnel operational controls and readouts are provided at the console. These include control and readout of fan speed, control and readout of probe position, ceiling height controls and limit switch indicator lights, and pressure controls for the ceiling seal. For convenience, approximately 6 m of extra cable makes the console somewhat portable.

4. THE LABORATORY AND INSTRUMENTATION

4.1 The Laboratory

The floor plan of the Fluid Modeling Facility is shown in Figure 21. The laboratory occupies approximately 1860 m² (20,000 ft²) of floor space. The main floor area contains the Meteorological Wind Tunnel, the Water Channel/Towing Tank (to be described in a separate report) and an Instrument Calibration Wind Tunnel used for small scale experiments and calibration of meteorological wind instruments.

A wood and metal working shop contains tools and equipment for the construction of detailed models from wood, metal, and plastics. Minor modifications, repairs and additions to the facility are also performed in-house. An electronics shop is used for the repair and maintenance of instruments and other electronic equipment and for the development of new instrumentation. A photographic darkroom is available for processing black and white films and making prints.

4.2 The Minicomputer

A Digital Equipment Corporation PDP 11/40 minicomputer is located within the facility to sample, process and store all laboratory data. A block diagram of this system is shown in Figure 22. Its main components include a 16-channel, 12 bit analog-to-digital converter, a PDP 11/40 central processing unit with 80K words of memory, 3 disk drives, 3 magnetic tapes drives, several terminals (including a refresh-graphics terminal), and an electrostatic printer/plotter. Its operating system is RSX-11D which permits multiple tasks and multiple users to access the system simultaneously. Real-time analysis of the outputs of electronic data gathering instruments provides instant feedback to the experimenter on the results of data being taken. The refresh-graphics terminal allows the operator to display data graphically as it is acquired and to make decisions based upon data taken to date; e.g., is the velocity profile smooth or do additional points need to be taken?

The system as configured permits sampling rates up to a maximum of 1000 samples/s. It is programmed to carry running sums and sums of squares during sampling (in triple-precision arithmetic) so that, for example, the mean velocity, turbulence intensity, and Reynolds stress, are available immediately after the last sample has been acquired. The magnetic tape drives provide for storage of digitized data for later analysis, such as the computation of spectra or correlations.

4.3 Flow Measurement Apparatus

Velocity measurements in the wind tunnel are made with TSI constant temperature anemometers (Models 1054A and B are available). Hot-film (as opposed to hot-wire) sensors are used exclusively, as the higher frequency response of hot-wires is not necessary and the hot-films are much less fragile. Since hot-film anemometers do not directly measure the air speed, they must be calibrated in a known air stream. This is done by placing the hot-film sensor next to a pitot tube in the free stream flow in the wind tunnel and running the computer program HCALX. The air stream velocity is calculated from the differential pressure indicated by the pressure measuring device connected to the pitot tube, in general, an MKS Baratron model 170M electronics unit connected to a model 310BH-10 sensor head. This velocity is input to HCALX through the operator's terminal and the A/D converter samples the output voltage of the anemometer, typically at 500 samples/s for 15 s. After a sufficient number of calibration points (typically 6) are established over the velocity range of interest, HCALX then computes the best fit to King's law $E^2 = A + BU^\alpha$ (E is the output voltage of the anemometer, V is the mean velocity, and A , B , and α are constants to be determined). It steps α from 0.30 to 0.60 (in steps of 0.01), each time computing the best-fit A and B and each time retaining the least-squares error. When finished, it then searches for the best α , i.e., that which minimizes the least-squares error. A typical calibration curve is shown in Figure 23. Note that the zero-flow voltage is recorded, but is not used in the calculation of the best fit curve.

To make turbulence measurements in the wind tunnel, then, the best fit A , B , and α values from HCALX are input to another program called HOT, which generates one or more tables of digitized voltage versus velocity. During the sampling period, HOT samples the anemometer output, uses a

table look-up procedure for linearization (much more efficient than calculations), and carries the running sums of (1) the velocity indicated by each film, (2) the square of the velocity indicated by each film, and, if cross films, (3) the cross-product of the velocities indicated by each film pair. After the sampling is finished, HOT uses these sums to compute the mean velocity, the angle of the mean flow, the two turbulence intensity components, and the Reynolds Stress.

Because the hot-film is sensitive to ambient temperature changes, the room temperature is carefully monitored. If it changes by more than 0.5°C, the operator inputs the new temperature into HOT, in which case, a new look-up table is generated according to $E^2 = (A + B^\alpha) (T_f - T_{\text{new}}) / (T_f - T_{\text{cal}})$, where T_f is the film temperature, T_{new} is the new room temperature, and T_{cal} is the room temperature at which the sensor was calibrated.

4.4 Concentration Measurement Apparatus

Pollutant dispersion is studied by releasing a hydrocarbon tracer mixture from the model source, collecting samples through a sampling tube, and measuring the concentration of tracer in the sample. Tracers that have been used are methane and ethylene, being chosen for their buoyant and neutrally buoyant properties, respectively. Four Beckman model 400 Hydrocarbon Analyzers (flame ionization detectors, FID's) are used in the continuous operating mode to determine the concentration of tracer in the sample. The "zero" and "span" are adjusted on the FID using "zero" air (less than 1 ppm total hydrocarbons) and a 1% mixture of methane in air (or equivalent ethylene standards), respectively. The zero and span are checked after each concentration profile is obtained to be certain that the electronics has not drifted. The output of the FID is also processed by the minicomputer through the program HCA. The response time of this instrument (typically 0.5 s), however, is too large to obtain useful statistics on concentration fluctuations.

Because the wind tunnel is open-return, background hydrocarbons in the room air tend to increase during a testing period. To account for this shifting, background measurements are taken periodically during an experiment. The HCA program subtracts the background hydrocarbon concentration from the sample value by assuming a linear change of background with time between readings.

5. PERFORMANCE CHARACTERISTICS OF THE WIND TUNNEL

5.1 Calibration of Empty Tunnel

The basic performance characteristics of the empty wind tunnel, with the ceiling adjusted parallel to the floor, are presented in this section. A series of tests was undertaken to examine the steadiness, uniformity and turbulence intensity of the core flow and the growth of the sidewall boundary layers. The first tests investigated the steadiness of the flow.

Very low frequency fluctuations in flow speed, i.e., over the order of a minute or longer, are referred to as drift. Drift can result, for example, from changes in line voltage, gradual changes in air temperature, from "hunting" in the fan speed controller, etc., but has never been a problem with the MWT. Velocity fluctuations faster than a few hertz and generally associated with rotational motion are called turbulence and will be discussed later. Surging, as defined here, refers to fluctuations in flow speed in a middle-frequency band, in the range of 2 to 60 cycles per minute. It is generally associated with separation somewhere in the wind tunnel circuit and is most easily identified as irrotational motion, i.e., two velocity sensors placed in the test section will show nearly perfect correlations in fluctuations regardless of their separation distance or direction with respect to one another.

Initial tests in the MWT showed surging to be a problem, annoying and bothersome when attempting to obtain time averages of velocity, etc. The surging amounted roughly to sinusoidal variations in speed, with peak amplitudes of approximately $\pm 3\%$ of the mean (1% rms) and frequencies roughly proportional to velocity. An example of the surging is shown in Figure 24.

Probing various parts of the circuit with smoke wands and attaching wool tufts to the sidewalls revealed separation in the diffuser downstream of the fan. The separation was undoubtedly caused by the large divergence angle of the diffuser. The problem was easily solved as mentioned in

Section 3, by installing a trip ring that forced separation to occur at the entrance to the diffuser. The trip ring reduced variations in speed to under 1% peak-to-peak values (under 1/2% rms). It reduced the top speed of the tunnel by approximately 3% (see Figure 24).

The tunnel was then calibrated, i.e., flow speed was determined as a function of fan speed. Figure 25 shows the results. Speeds above 1.2 m/s were determined using a standard Pitot tube and micromanometer. Lower speeds were obtained by timing smoke puffs. The data in the figure show the wind speed, for all practical purposes, to be directly proportional to fan speed. Although the design speed of 8 m/s was not obtained with the present blade pitch angle, it could easily be exceeded in a matter of a few minutes by increasing the pitch angle, since the motor is taxed to only 70% of its capacity with the present adjustment. The flow is quite steady at all speeds, including those below 1 m/s.

Velocity surveys were made with a TSI Model 1054A anemometer and a 1210-20 hot-film probe. Signals from the anemometry were processed in real time on the minicomputer, as discussed in Section 4, except that during this period of time, the operating system was RT-11, a single task, single user system allowing sampling rates up to 6000 hertz. A suppression was applied to the bridge voltage fed to the minicomputer to produce a signal within the range of the A/D converter; the turbulence intensities presented here thus represent total fluctuations - including drift and surging - since low frequency fluctuations were not filtered out as is conventionally done. Generally, one minute samples were used to form time averages and sampling rates were 2000 samples/s, which is far beyond the Kolmogorov frequency. Surveys were made at 3 wind speeds and at 3 downstream locations, representing the entrance, middle and downstream end of the test section. Turbulence intensities were normalized with the local mean velocity.

Lateral (cross-stream horizontal) profiles of mean velocity and turbulence intensity at a nominal velocity of 1.5 m/s are presented in Figure 26. Figure 27 presents the vertical profiles of mean velocity and turbulence intensity. The mean velocity in the core, i.e., outside the sidewall boundary layers, is uniform to within $\pm 2\%$ of the mean at any given section. The core flow accelerates by approximately 7% over

the length of the test section because of the growth of the wall boundary layers. The core flow can be made to be nonaccelerating by adjustment of the ceiling height, but it was not attempted in this case. The turbulence intensity, nominally 0.5%, would not be considered low for a high-performance aeronautical wind tunnel, but may be considered excellent for an ultra-low-speed meteorological wind tunnel.

Figures 28 and 29 show the development of the boundary layers along the floor of the test section at 3 and 6 m/s respectively. It may be of interest to note that the boundary layer thicknesses are well-predicted by

$$\delta = \frac{0.376 x}{Re_x^{1/5}}$$

where δ is the boundary layer thickness ($U = 0.99 U_\infty$), x is the distance from the entrance of the test section, and Re_x is the local Reynolds number, $U_\infty x / \nu$. The above formula is, of course, the standard textbook formula for the growth of a turbulent boundary layer over a flat plate.

5.2 Development of Two-Meter-Thick Boundary Layer

The simulation of atmospheric dispersion in a wind tunnel is especially difficult. In order to model buoyant plumes, it is desirable to use the largest convenient model scale (Snyder, 1972b), and hence, the thickest possible boundary layer. It is also desirable to develop this thick boundary layer in as short a fetch as possible and to maintain this boundary layer in an equilibrium state over the region of interest downstream of the source. Finally, it is important that the otherwise undisturbed boundary layer be two-dimensional.

The aim in this first development of a simulated atmospheric boundary layer was to obtain something representative of neutrally stable flow over rural terrain, say, somewhere between open country and woodland forest. The boundary layer to be simulated was to have the following approximate properties (Davenport, 1963; Counihan, 1975):

$$\begin{aligned} \text{Boundary layer thickness, } \delta &\approx 600 \text{ m} \\ \text{Profile Shape, } U/U_\infty &= (z/\delta)^{1/6} \end{aligned}$$

Roughness length, $z_0 \approx 30$ cm
Scale Factor ≈ 300

The generator system chosen was a slight modification of that developed by Counihan (1969). The elliptic wedge vortex generators and castellated barrier were scaled versions of Counihan's: the height, H , of the generators was 1.83 m; their length in the streamwise direction was $H/2$; their spacing was $H/2$; the distance from the castellated barrier to the front edge of the generators was $5H/6$; the barrier height between castellations was $H/7$; the height of the top of the castellations was $H/5$; the castellations were aligned with the center lines of the generators; the tunnel height was $7H/6$; and the distance from the test section entrance to the barrier was $H/3$. Four generators were spaced across the test section such that the centerline of the wind tunnel was mid-span between generators. However, the roughness elements differed from those of Counihan. Two-dimensional roughness elements were used to maintain the boundary layer in equilibrium. They consisted of wooden strips $H/100$ (0.019 m) in height and $H/36$ (0.051 m) wide and were spaced $H/4$ (0.475 m) apart along the floor of the test section perpendicular to the flow direction. Figure 30 provides a sketch of this vortex generator system.

Measurements described here were taken as described in Section 3; the sampling rate was 800 Hz and the averaging time was 1 min. Unless otherwise noted, all measurements were made at a freestream velocity of 3 m/s.

The development of the mean velocity profile along the centerline of the wind tunnel is shown in Figure 31. These measurements were made over a period of approximately six weeks using both standard straight film probes (TSI Model 1210-20) and x-film probes (TSI Model 1243-20). The agreement between the data taken with the two types of probes is regarded as excellent. The mean velocity profile is seen to be unchanging over the range of $4.5H < x < 7.5H$, and to be approximated very closely by a $1/6$ th power law, as desired. The data at $x = 6H$ at twice the wind speed show the flow to be essentially Reynolds number independent over the range $3\text{ m/s} < U_\infty < 6\text{ m/s}$. Some less extensive measurements reported earlier (Snyder and Lawson, 1976) showed a $1/5$ th power law at $U_\infty = 1.5\text{ m/s}$, but this difference is not regarded as significant. Finally, the measurements at $x = 8H$ are slightly different from those at $x = 7.5H$. The former are probably influenced by the proximity to the acoustic

silencers at the downstream end of the test section, since $x = 8H$ is only a few centimeters from the silencers.

The mean velocity profiles plotted in the log-law form in Figure 32 were used to define the aerodynamic characteristics of the surface:

$$\frac{U}{u_*} = \frac{1}{k} \ln\left(\frac{z - d}{z_0}\right)$$

where u_* is the friction velocity, d is the displacement height, and k is the von Karman constant (0.4). The displacement height was found to be negligible. Within the precision of the measurements, the roughness length is found to be 0.65 mm (0.00036H), and invariant with respect to position or wind speed. Note that the depth of the logarithmic portion of the boundary layer is approximately 0.15H. The roughness length of the prototype boundary layer would be 20 cm, slightly less than the desired value. According to Counihan (1975), this roughness length would correspond to moderately rough terrain, say, agricultural/rural, and would yield a power law index of approximately 1/6th, which fits the data quite well.

The development of the longitudinal and vertical turbulence intensities and Reynolds stresses are shown in Figures 33, 34, and 35, respectively. These turbulence quantities have been normalized by the free-stream velocity U_∞ . Again, these data were obtained over a period of approximately 6 weeks using both straight-film and x-film probes. The repeatability of the measurements is regarded as excellent. The figures show the streamwise development to consist of a slight decay above $z/H = 0.15$. Evidently, the flow close to the surface is nearly in equilibrium with the surface, i.e., the roughness is matched reasonably well to the barrier height (Robins, 1975). Notice that the turbulence intensity and nondimensional stress profiles are only very slightly affected by changing the wind speed.

Counihan's (1969) data at $x = 4.5H$ are reproduced on the figures for comparison. The agreement is reasonably good considering that Counihan's estimated roughness length was proportionately twice as large. Whereas surface values of turbulence intensities and Reynolds stress are matched very closely, the present measurements show a more rapid decrease with height and hence lower values up to approximately $z/H = 0.4$. These differences are probably due to the different character of the roughness (two-dimensional)

and to the lower value of roughness length.

The constant stress layer is at most 10% of the boundary layer depth. The surface stress, approximately $0.0022 U_\infty^2$, is essentially independent of position; its magnitude is consistent with that obtained from the log-linear plot of the mean velocity profile in Figure 32. It is also very close to the proposed curve of Counihan (1975) for $z_0 = 20\text{cm}$ ($\overline{u'w'} = 0.0023 U_\infty^2$). The longitudinal turbulence intensity at an equivalent full-scale height of 30 m, however, is somewhat lower than that proposed by Counihan (1975). The proposed value is 17%; the present value is approximately 14%. Finally, in the surface layer, the ratio of vertical to longitudinal turbulence intensities is 0.50, compatible with previously reported values (Counihan, 1975).

The Reynolds stress measurements (Figure 35) show considerable scatter, which is due at least in part to an insufficient averaging time. It is difficult to discern any trends amidst the scatter except possibly a decrease in the stress with downstream distance at mid-elevations.

The lateral homogeneity of the flow is examined in Figures 36 through 39. The mean velocity (Figure 36) is seen to be within $\pm 5\%$ of the mean for any given horizontal plane. The turbulence intensities (Figures 37 and 38) show wider deviations. Aside from the decay of turbulent energy with downstream distance, the turbulence intensities may be judged as reasonably homogeneous at any given section, i.e., deviations from the mean turbulence intensity at any given plane are within $\pm 10\%$ in the middle and lower portions of the boundary layer and within $\pm 20\%$ at the upper levels (where the "mean" turbulence intensity is typically only 2 to 3%).

The Reynolds stress measurements (Figure 39) show very large scatter, typically $\pm 50\%$. The lateral deviations in stress appear to be vestiges of the fins at the highest elevations, but do not appear to be correlated directly with the existence of the fins in the middle and lower portions of the boundary layer. The deviations from the mean appear to diminish and the stress appears to become more laterally homogeneous as the flow develops (although very slowly).

On the whole, the measurements of the boundary layer structure at $x/H = 4.5$ compare quite favorably with those measured by Counihan (1969). The boundary layer is seen to undergo a very slow streamwise development as was also noted by Castro et al. (1975). The most disturbing aspect of this

boundary layer is the lateral nonuniformity of the Reynolds stress. Figure 39 shows much wider deviations from the mean than have been reported previously. However, the previous measurements have not examined variations across the entire width of the wind tunnel; instead, they have typically measured only three vertical profiles: one on the generator centerline, one at midpoint between two generators (midspan), and one halfway between those two (quarter-span). It is perhaps only fortuitous that previous investigators have found such a high degree of lateral uniformity in their Reynolds stress measurements.

The streamwise development of the boundary layer is similar to that observed by Castro et al. (1975); it is mainly a decay in the turbulence levels in the regions $z/H > 0.15$. Contrary to the results of Castro et al., however, slight differences in vertical turbulence intensity and Reynolds stress were observed at different wind speeds. Hence, this boundary layer is not entirely Reynolds number independent. The roughness used by Castro et al. was much larger than the present roughness; they mentioned that initial work had been done with smaller roughness and that a Reynolds number dependent flow had been obtained.

Measurements of plume dispersion were made in this boundary layer to determine whether its dispersive characteristics were similar to accepted atmospheric dispersion characteristics. A model stack of height $0.2H$ emitted a neutrally buoyant effluent of a 1% mixture of methane in air. The ratio of effluent speed to wind speed was maintained at 1.5 to avoid downwash in the wake of the stack. Lateral and vertical concentration profiles through the plume centerline were measured at three positions downwind, as shown in Figures 40 and 41, along with "best fit" Gaussian curves. The lateral and vertical standard deviations of plume spread are plotted along with Pasquill-Gifford curves for stabilities B, C, D, and E (Turner, 1967) in Figure 42. Vertical dispersion within the wind tunnel boundary layer is closest to stability C (slightly unstable), whereas the horizontal dispersion is closest to stability D (neutral). The comparison with "accepted" atmospheric data is regarded as good. These results are fairly typical of other comparisons of wind tunnel measurements with Pasquill-Gifford curves, cf. Robins (1978) or Wilson and Netterville (1978). The lower slopes of the σ versus x curves from the wind tunnel are also typical of other wind tunnel results (ibid,

above references) and result from the slowly decaying wind tunnel turbulence and possibly, in the case of the lateral spread, from the inability of the wind tunnel to simulate the low frequency fluctuations in wind direction and wind direction shear. Even though the turbulence structure is developing somewhat with downstream distance and the Reynolds stress measurements show rather gross nonuniformities, this boundary layer may be acceptable for a number of purposes. It may safely be used for short range diffusion studies, for example, for comparison types of studies where the object is to determine building downwash effects from a short, nearby stack. It should obviously not be used for longer range studies, where the plume width would be a substantial fraction of the tunnel width, without further testing.

More recent experiments with a trip fence and gravel roughness have shown a much more laterally uniform boundary layer. A report on this new boundary layer with much more extensive measurements and analysis is forthcoming.

REFERENCES

- Bradshaw, P. and Pankhurst, R., 1964: The Design of Low-Speed Wind Tunnels, Prog. Aero. Sci., v. 5, p. 1-69.
- Castro, I.P., Jackson, N.A. and Robins, A.G., 1975: The Structure and Development of a 2m Simulated Suburban Boundary Layer, Central Electricity Generating Board, Res. Dept., Marchwood Engrg. Lab., R/M/N800, March.
- Counihan, J., 1975: Adiabatic Atmospheric Boundary Layers: A Review and Analysis of Data from the Period 1880-1972, Atmos. Envir., v. 9, no. 10, p. 871-905, Oct.
- Davenport, A.G., 1963: The Relationship of Wind Structure to Wind Loading, Paper 2, Proc. Conf. on Wind Effects on Bldgs. and Structures, Nat. Phys. Lab., June, HMSO, London, 1965, p. 54-102.
- Davis, G., 1957: Non-uniform Flow through Wire Screens, Ph.D. Dissertation, Univ. of Cambridge.
- Pankhurst, R.C. and Holder, D.W., 1952: Wind-Tunnel Technique, Pitman and Sons, London.
- Pope, A. and Harper, J.J., 1966: Low-Speed Wind Tunnel Testing, John Wiley and Sons, Inc., NY., 457p.
- Robins, A.G., 1975: Wind Tunnel Modeling of Plume Dispersal, Central Electricity Generating Board, Research Dept., Marchwood Engrg. Labs., Mech. Research Memo. No. 236, Dec.
- Robins, A.G., 1978: Plume Dispersion from Ground Level Sources in Simulated Atmospheric Boundary Layers, Atmos. Envir., v. 12, no. 5, p. 1033-44.
- Snyder, W.H., 1972: Fluid Models for the Study of Air Pollution Meteorology: Similarity Criteria, Facilities, Review of Literature, and Recommendations, Unpublished.
- Snyder, W.H., 1972: Similarity Criteria for the Application of Fluid Models to the Study of Air Pollution Meteorology, Bound. Layer Meteorol., v. 3, no. 2, p. 113-34.
- Snyder, W.H., 1974: Fluid Modeling Facilities for the Study of Air Pollution Meteorology, Unpublished.
- Snyder, W.H. and Lawson, R.E., Jr., 1976: Determination of a Necessary Height for a Stack Close to a Building - A Wind Tunnel Study, Atmos. Envir., v. 10, no. 9, p. 683-91.
- Sundaram, T.R. and Ludwig, G.R., 1970: Simulation of Small-Scale Atmospheric Turbulence in a Laboratory Facility, Pres. at Subsonic Aerodyn. Testing Assoc. Mtg., Ottawa, Canada, May 14-15.
- Turner, D.B., 1967: Workbook of Atmospheric Dispersion Estimates, PHS Pub. no. 999-AP-26.
- Wilson, D.J. and Netterville, D.D.J., 1978: Interaction of a Roof-Level Plume with a Downwind Building, Atmos. Envir., v. 12, no. 5, p. 1051-59.



Figure 1. Overview of the EPA Meteorological Wind Tunnel.

REFERENCES

- Bradshaw, P. and Pankhurst, R., 1964: The Design of Low-Speed Wind Tunnels, Prog. Aero. Sci., v. 5, p. 1-69.
- Castro, I.P., Jackson, N.A. and Robins, A.G., 1975: The Structure and Development of a 2m Simulated Suburban Boundary Layer, Central Electricity Generating Board, Res. Dept., Marchwood Engrg. Lab., R/M/N800, March.
- Counihan, J., 1975: Adiabatic Atmospheric Boundary Layers: A Review and Analysis of Data from the Period 1880-1972, Atmos. Envir., v. 9, no. 10, p. 871-905, Oct.
- Davenport, A.G., 1963: The Relationship of Wind Structure to Wind Loading, Paper 2, Proc. Conf. on Wind Effects on Bldgs. and Structures, Nat. Phys. Lab., June, HMSO, London, 1965, p. 54-102.
- Davis, G., 1957: Non-uniform Flow through Wire Screens, Ph.D. Dissertation, Univ. of Cambridge.
- Pankhurst, R.C. and Holder, D.W., 1952: Wind-Tunnel Technique, Pitman and Sons, London.
- Pope, A. and Harper, J.J., 1966: Low-Speed Wind Tunnel Testing, John Wiley and Sons, Inc., NY., 457p.
- Robins, A.G., 1975: Wind Tunnel Modeling of Plume Dispersal, Central Electricity Generating Board, Research Dept., Marchwood Engrg. Labs., Mech. Research Memo. No. 236, Dec.
- Robins, A.G., 1978: Plume Dispersion from Ground Level Sources in Simulated Atmospheric Boundary Layers, Atmos. Envir., v. 12, no. 5, p. 1033-44.
- Snyder, W.H., 1972: Fluid Models for the Study of Air Pollution Meteorology: Similarity Criteria, Facilities, Review of Literature, and Recommendations, Unpublished.
- Snyder, W.H., 1972: Similarity Criteria for the Application of Fluid Models to the Study of Air Pollution Meteorology, Bound. Layer Meteorol., v. 3, no. 2, p. 113-34.
- Snyder, W.H., 1974: Fluid Modeling Facilities for the Study of Air Pollution Meteorology, Unpublished.
- Snyder, W.H. and Lawson, R.E., Jr., 1976: Determination of a Necessary Height for a Stack Close to a Building - A Wind Tunnel Study, Atmos. Envir., v. 10, no. 9, p. 683-91.
- Sundaram, T.R. and Ludwig, G.R., 1970: Simulation of Small-Scale Atmospheric Turbulence in a Laboratory Facility, Pres. at Subsonic Aerodyn. Testing Assoc. Mtg., Ottawa, Canada, May 14-15.
- Turner, D.B., 1967: Workbook of Atmospheric Dispersion Estimates, PHS Pub. no. 999-AP-26.
- Wilson, D.J. and Netterville, D.D.J., 1978: Interaction of a Roof-Level Plume with a Downwind Building, Atmos. Envir., v. 12, no. 5, p. 1051-59.



Figure 1. Overview of the EPA Meteorological Wind Tunnel.

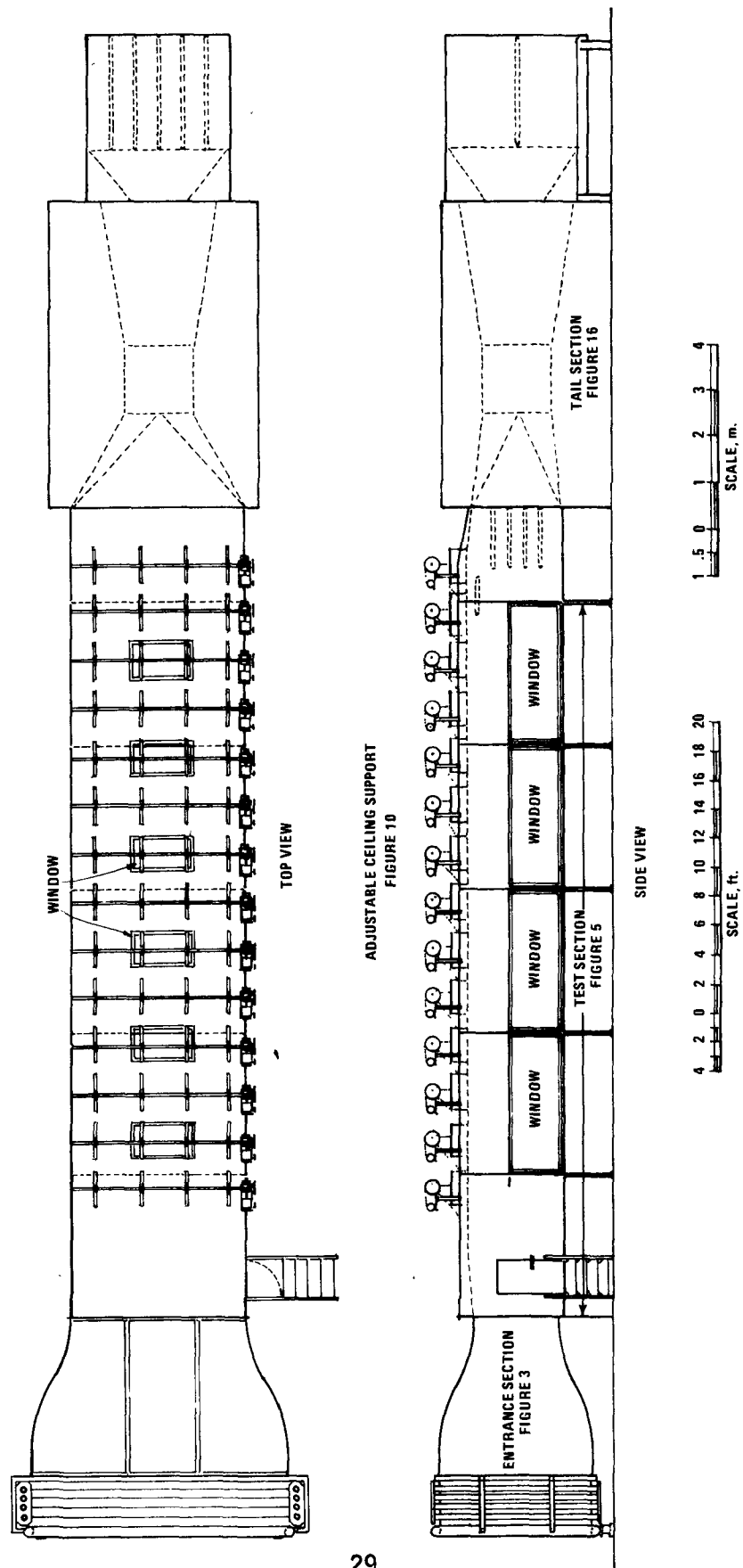


Figure 2. Overall plan and elevation of the EPA Meteorological Wind Tunnel.

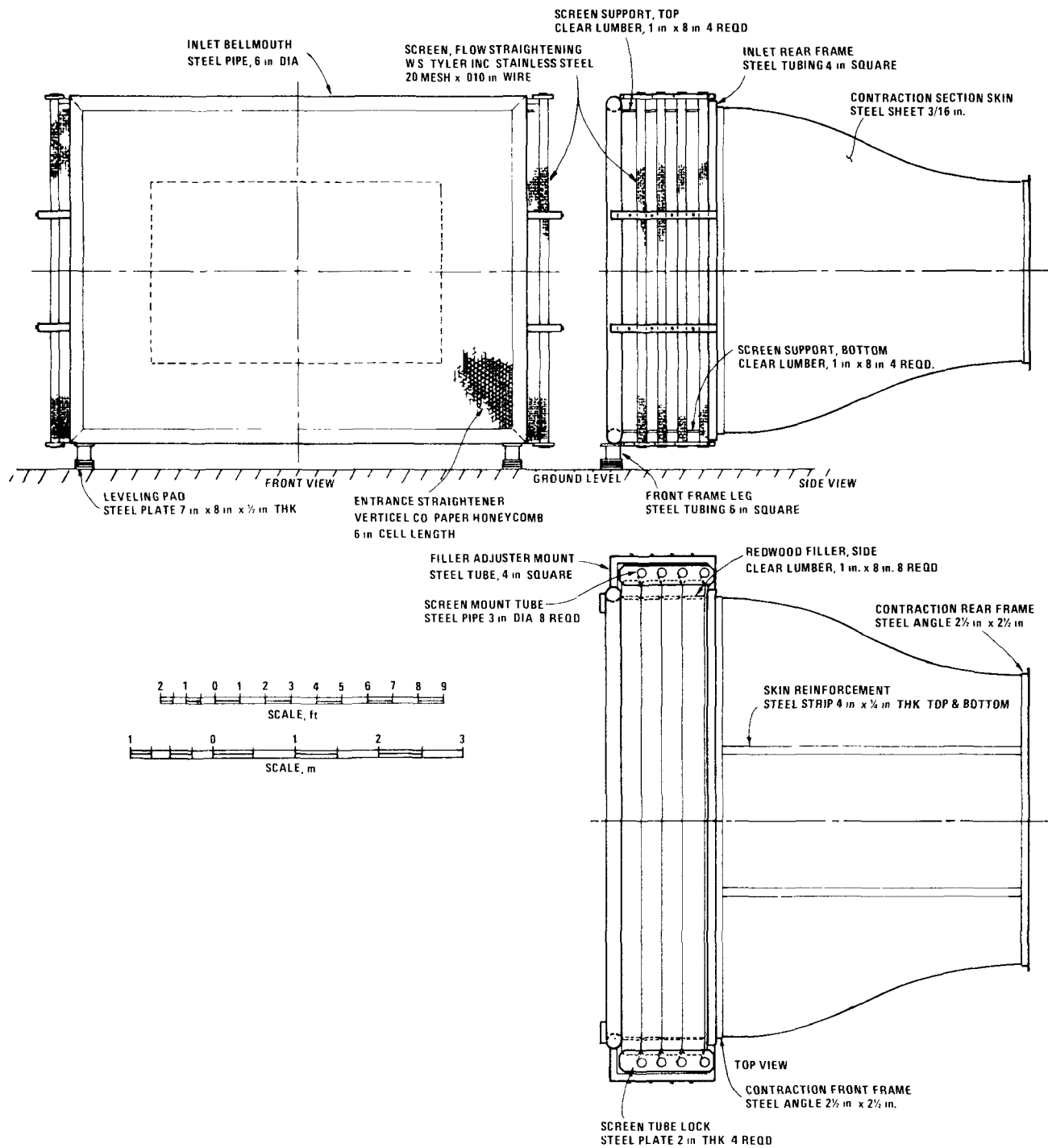
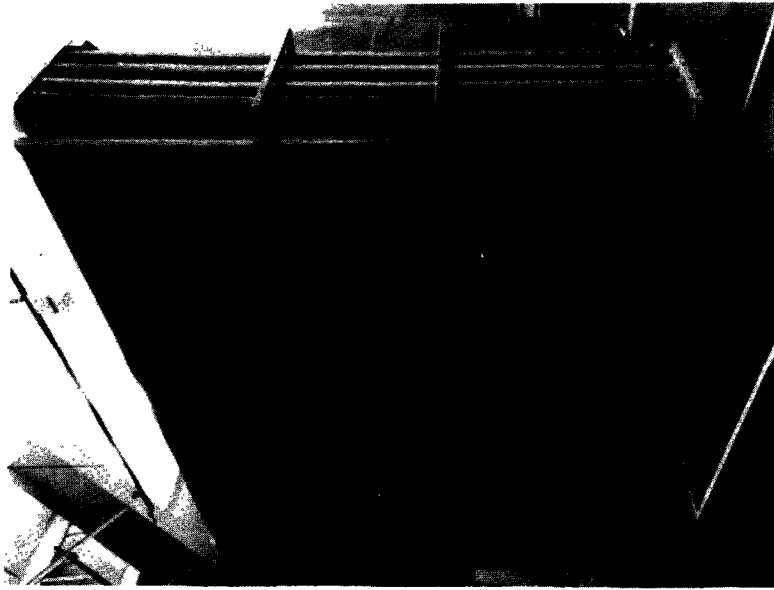


Figure 3. Front, side, and top views of entrance section.



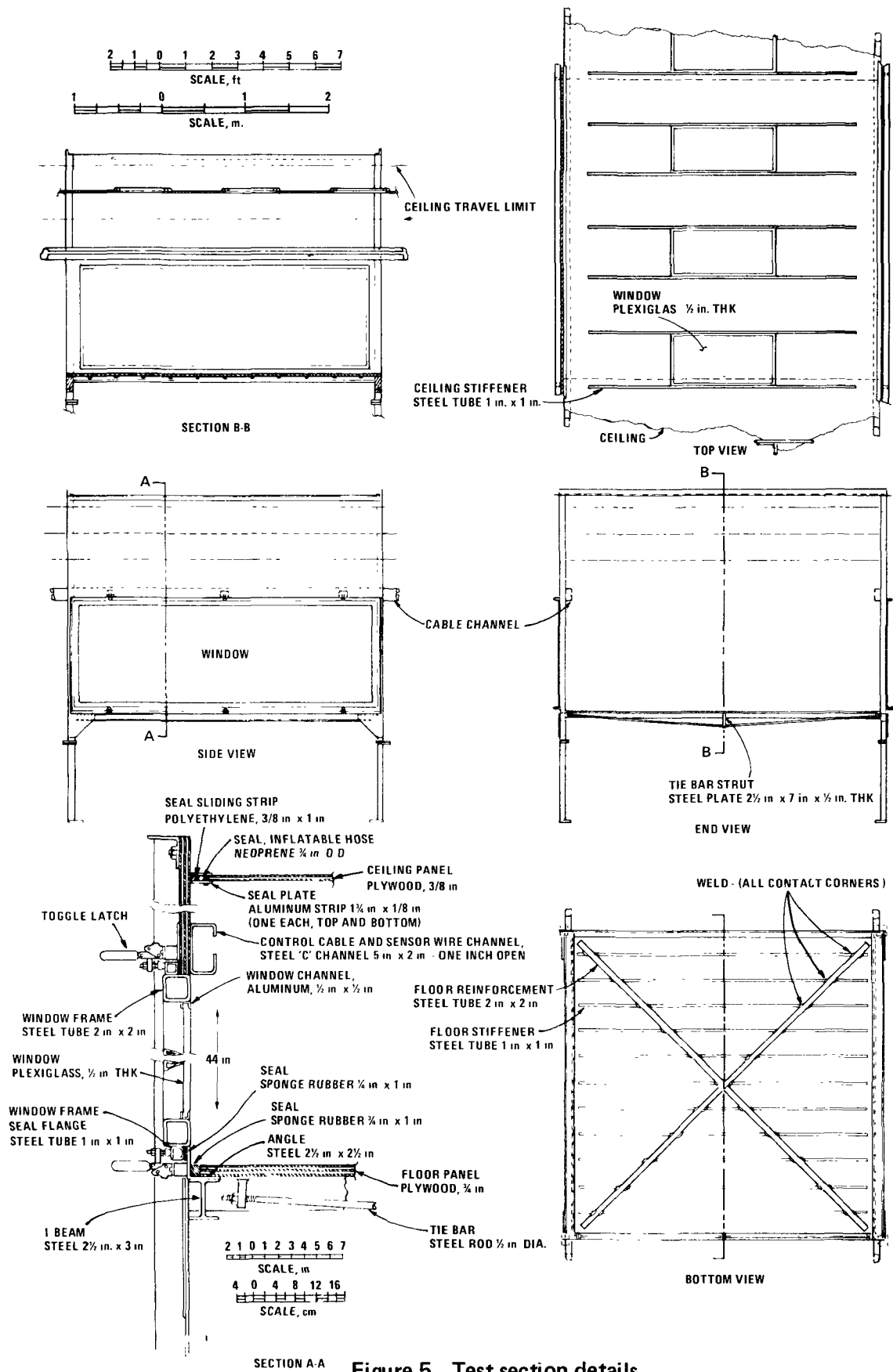


Figure 5. Test section details.

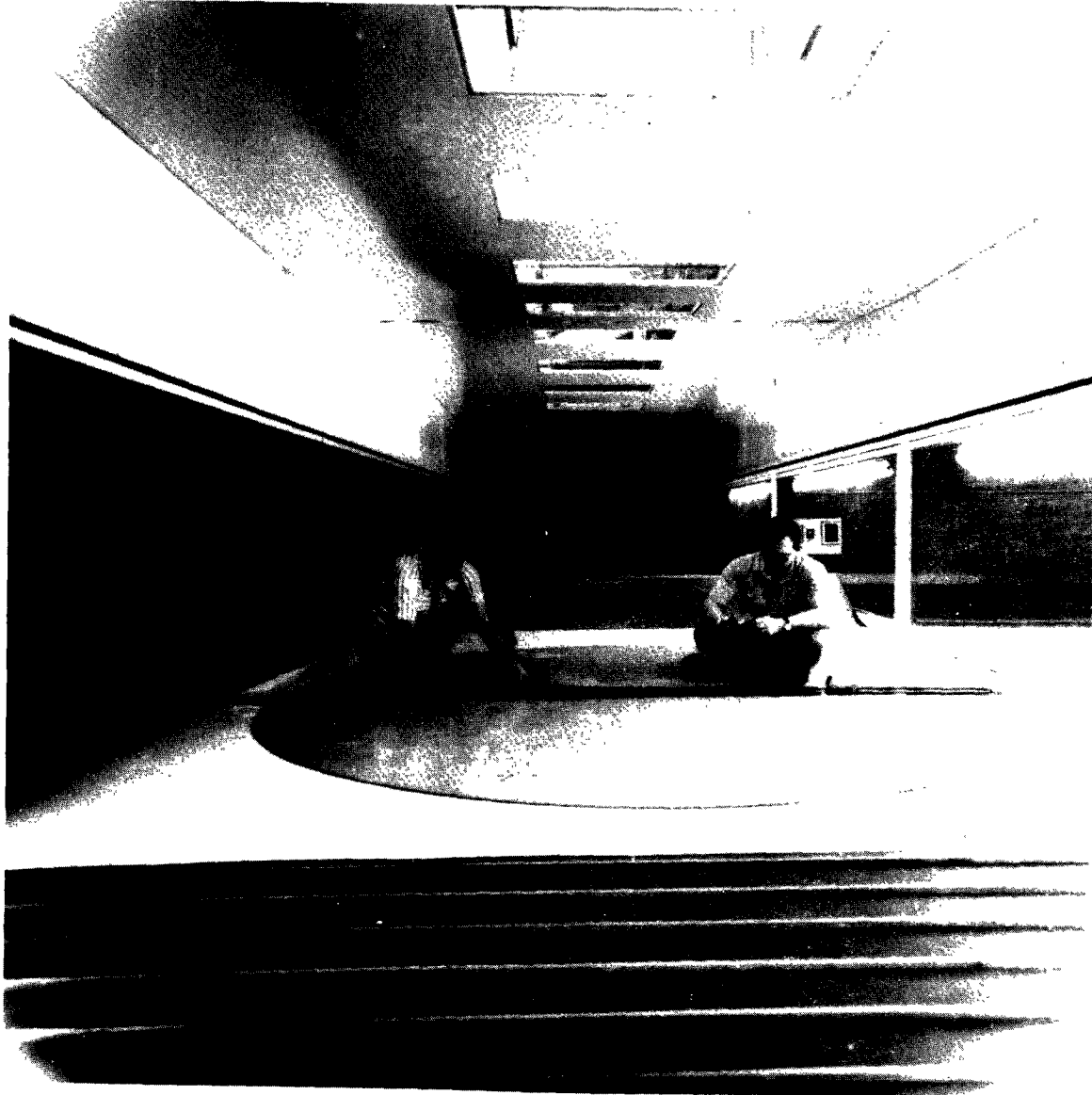


Figure 6. Inside view of test section looking downstream.

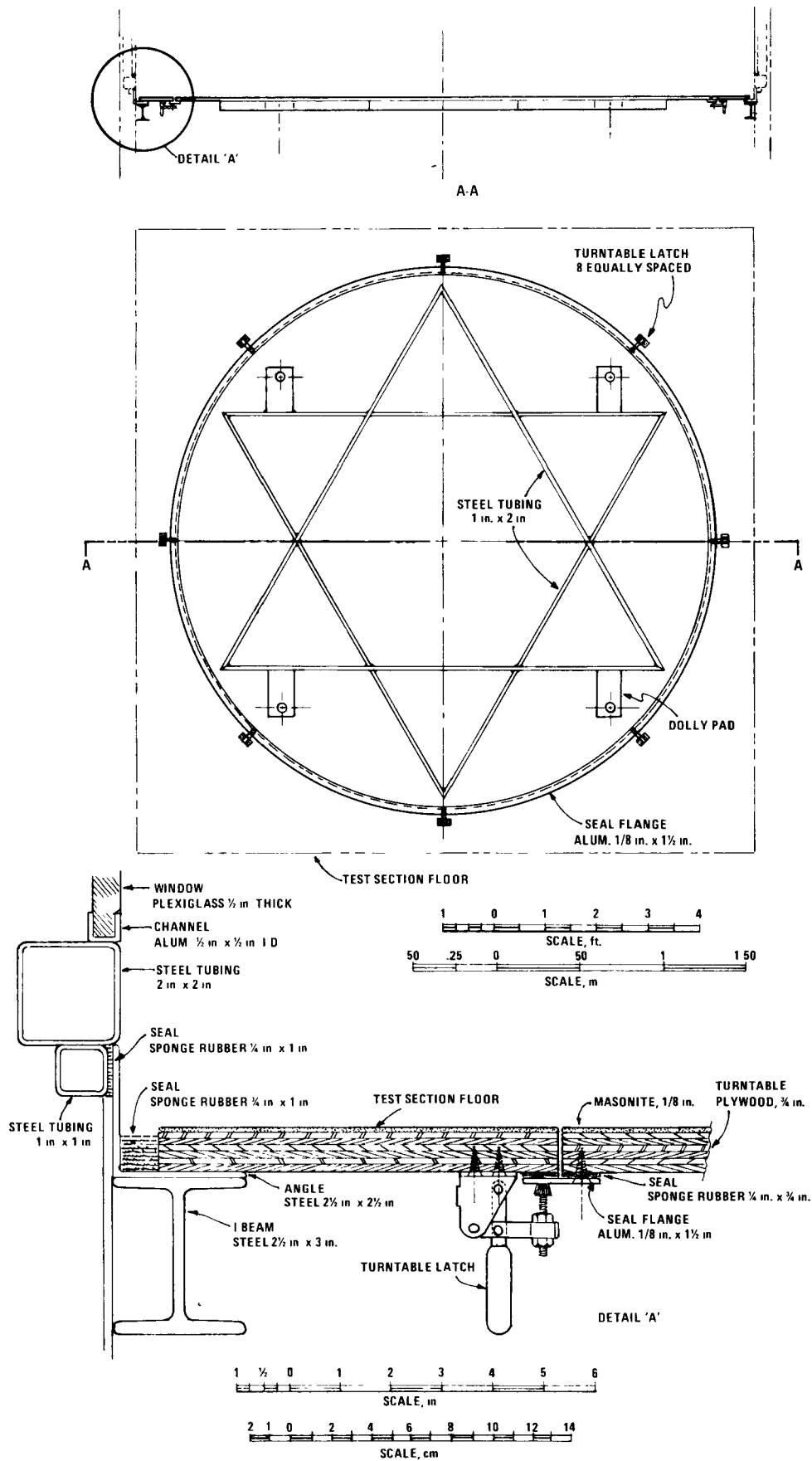


Figure 7. Turntable and details.

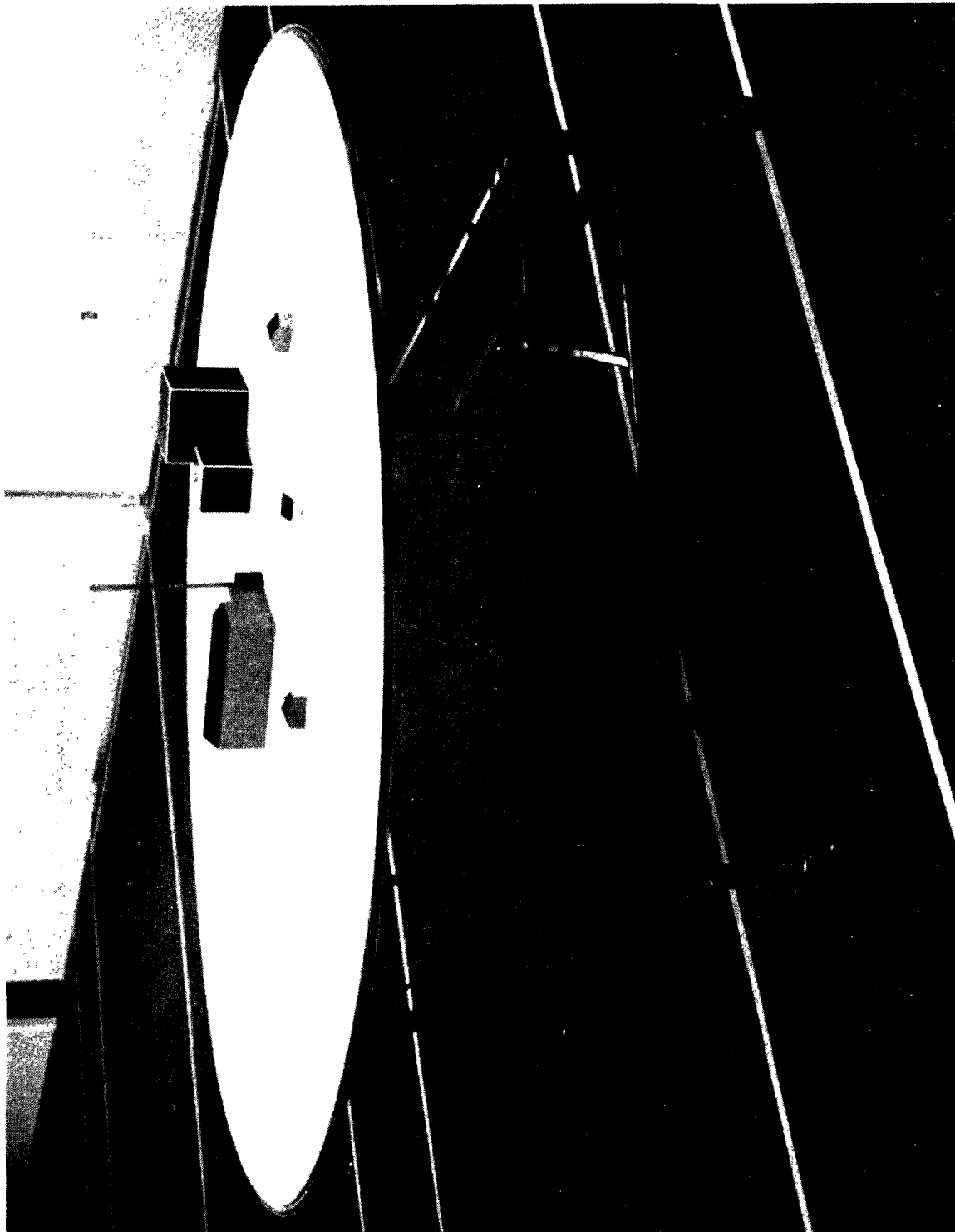


Figure 8. Turntable mounted on dolly.

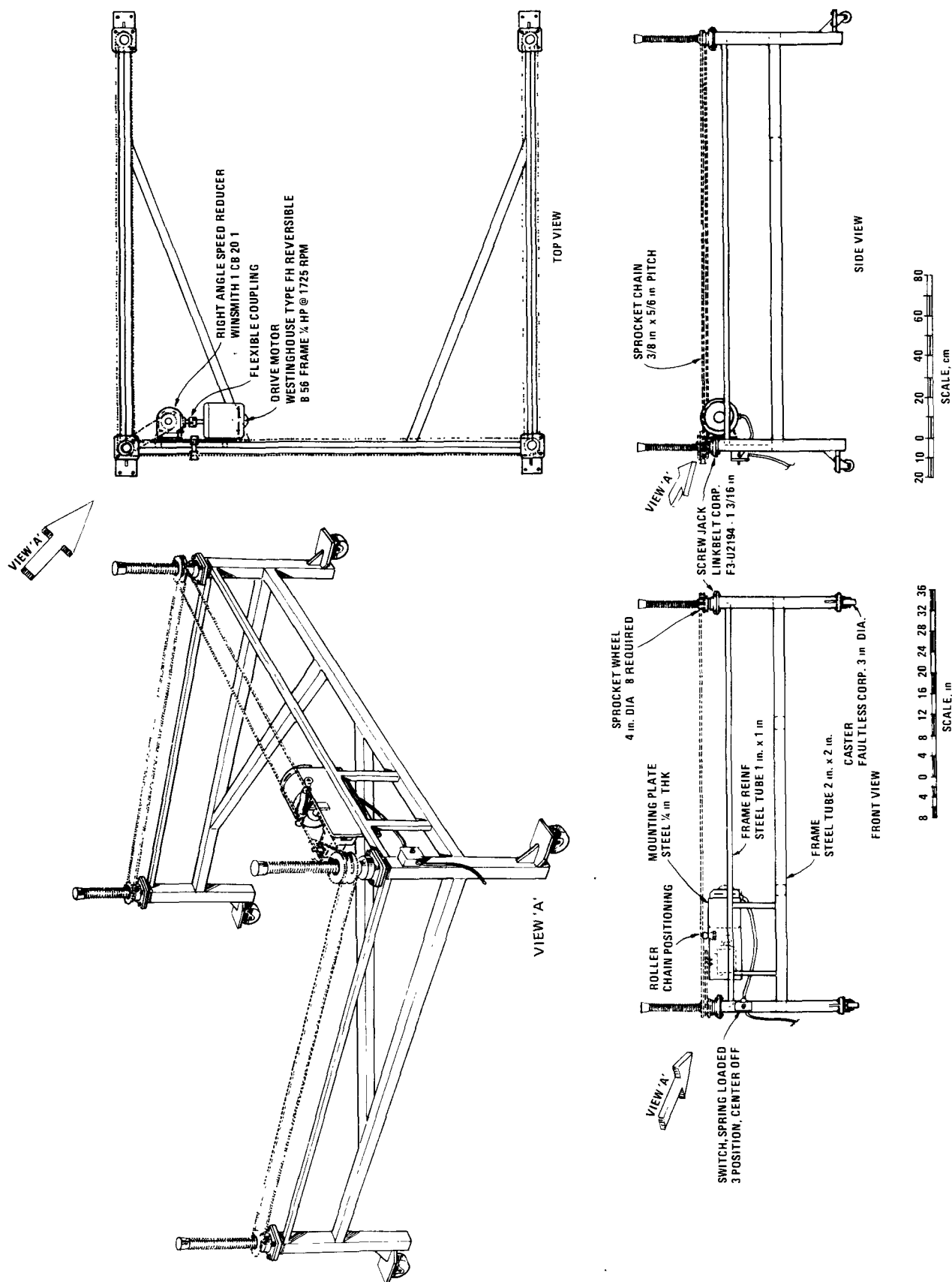


Figure 9. Turntable dolly.

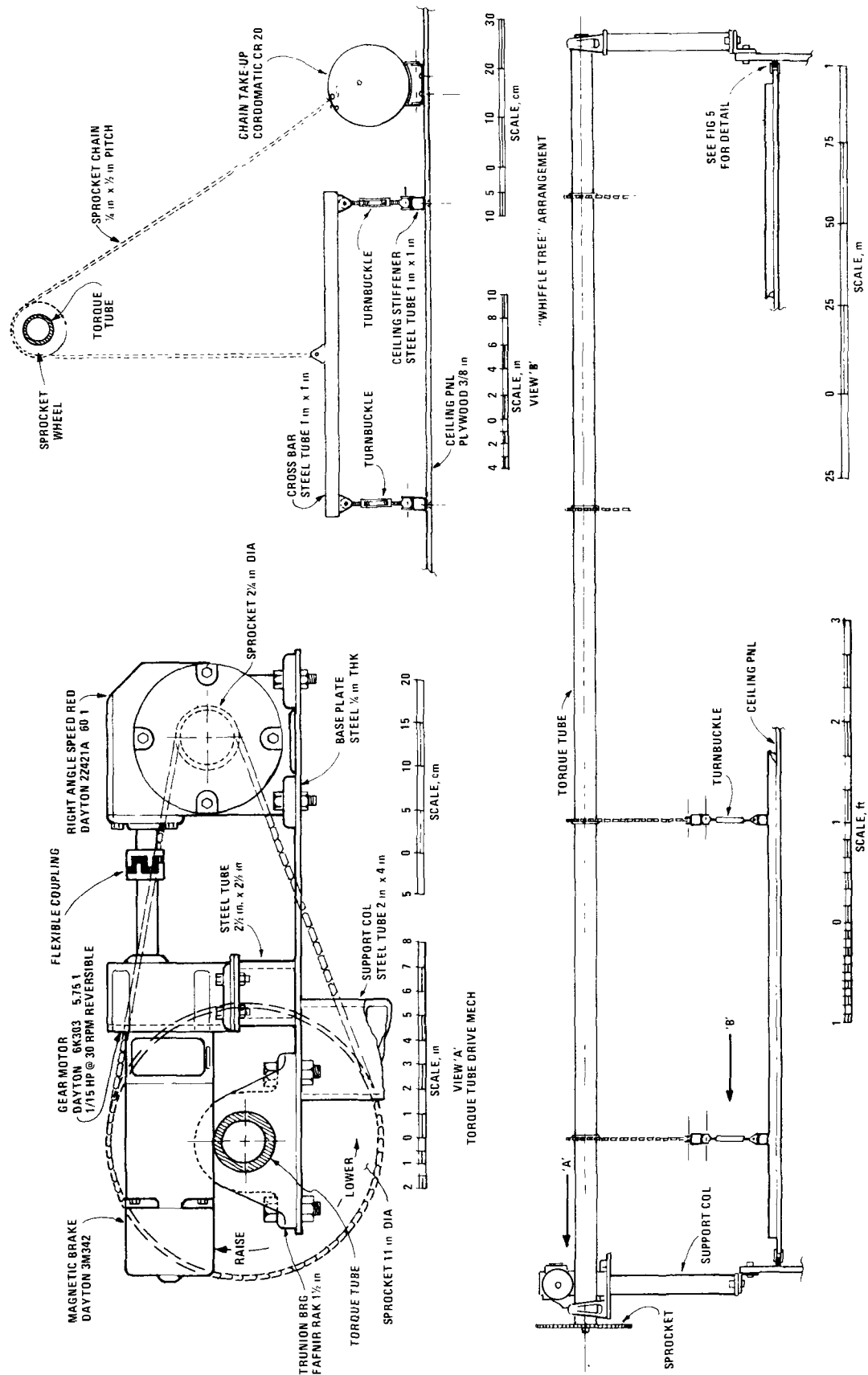


Figure 10. Details of adjustable ceiling support.

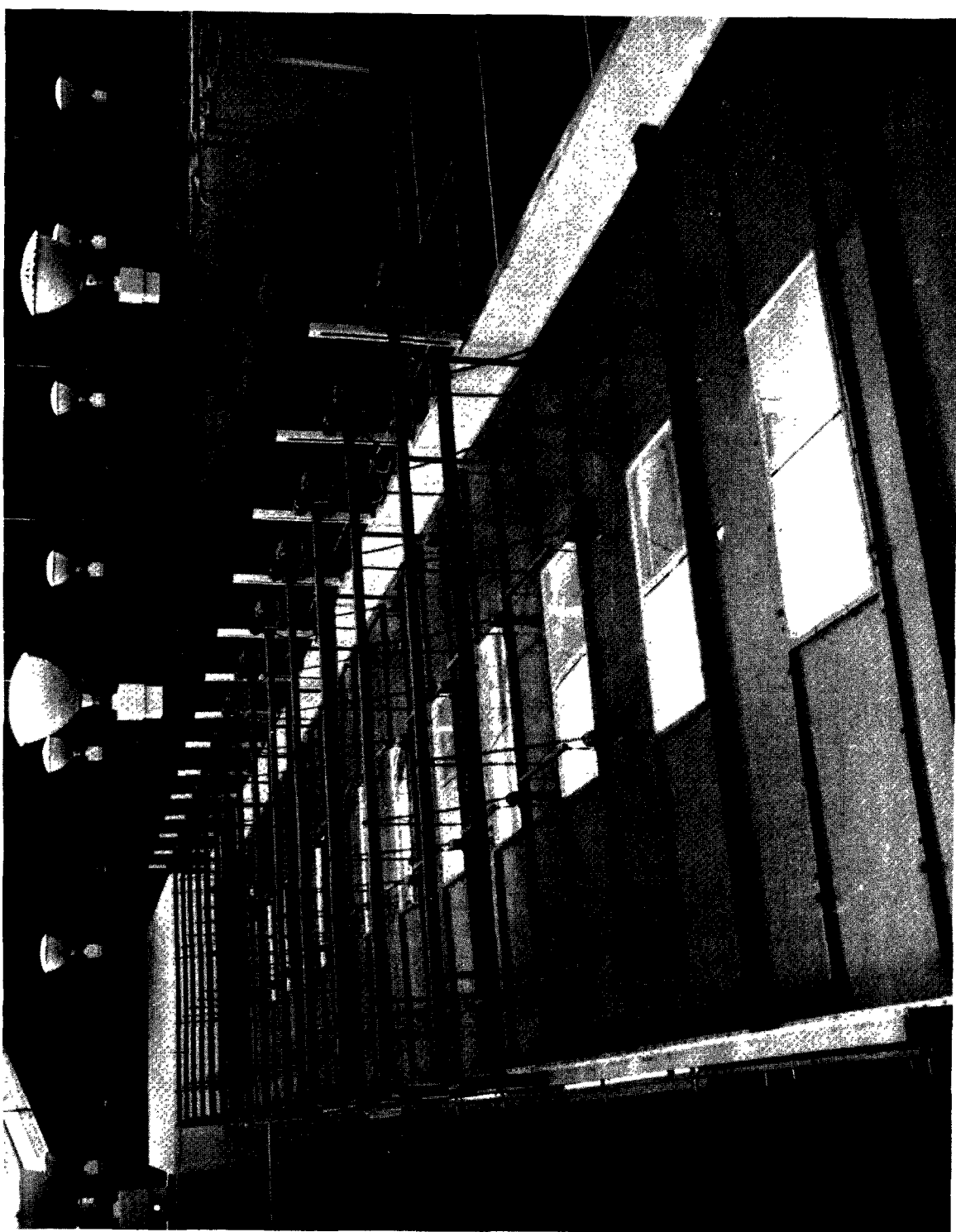


Figure 11. Overview of adjustable ceiling support.

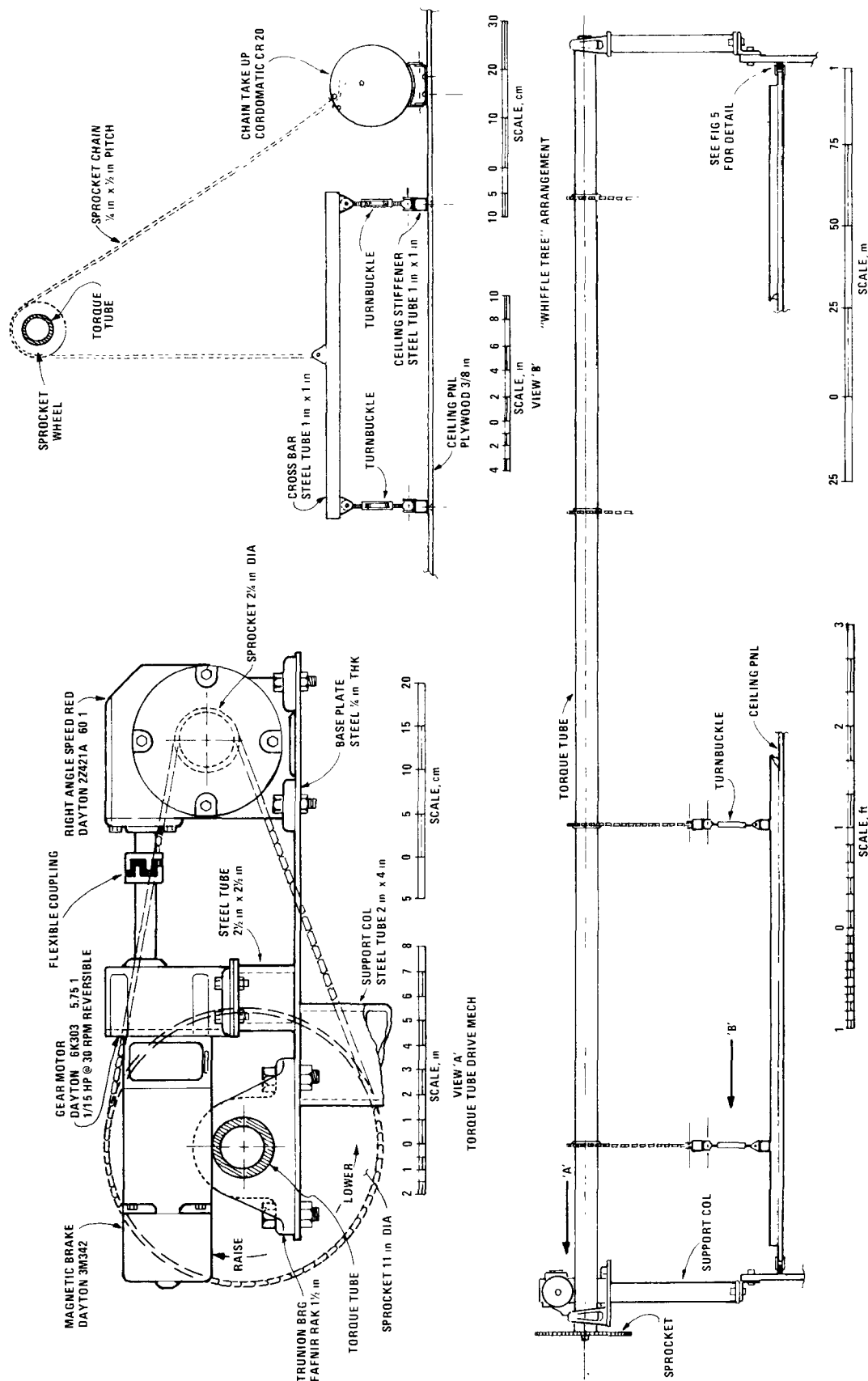


Figure 10. Details of adjustable ceiling support.

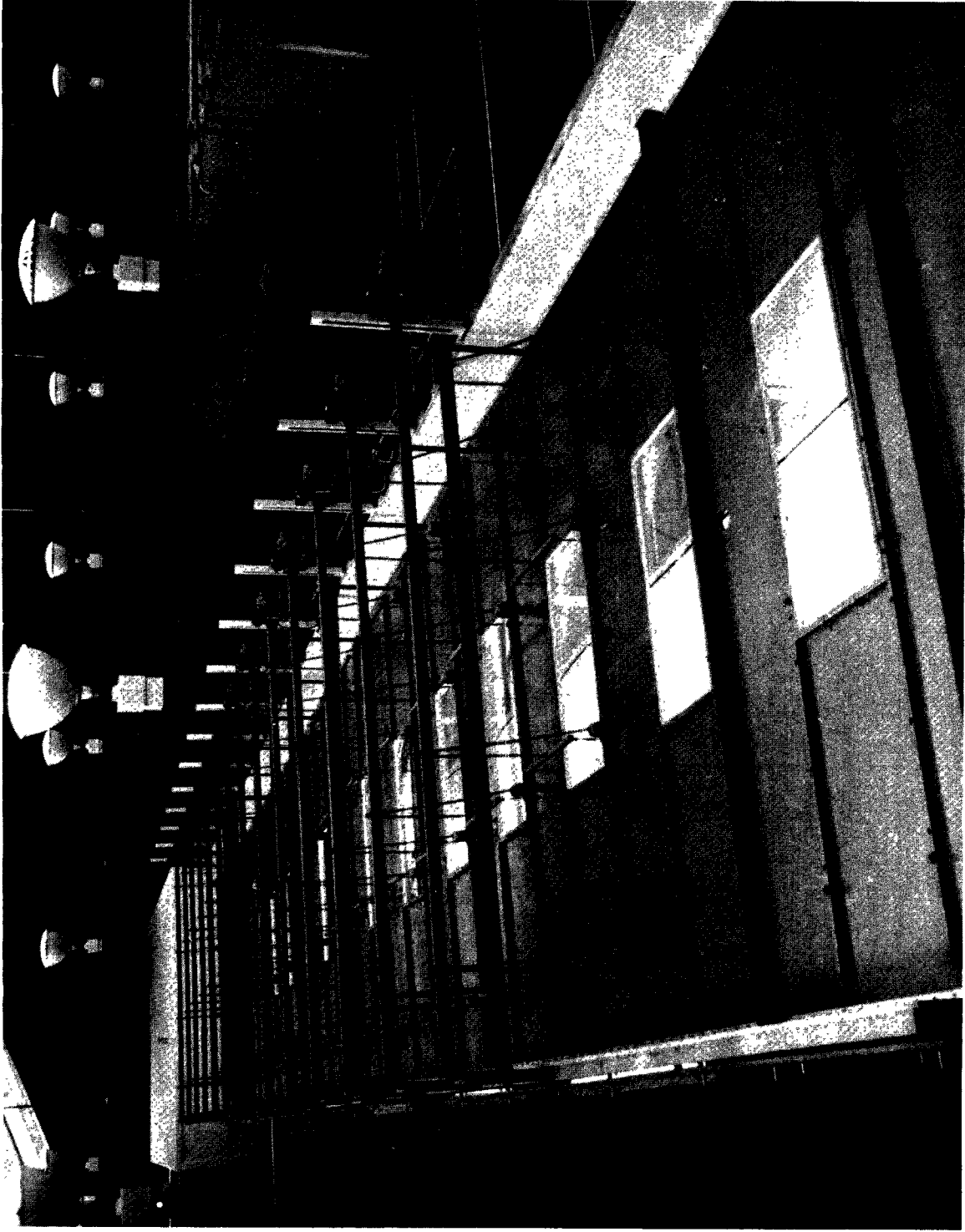


Figure 11. Overview of adjustable ceiling support.

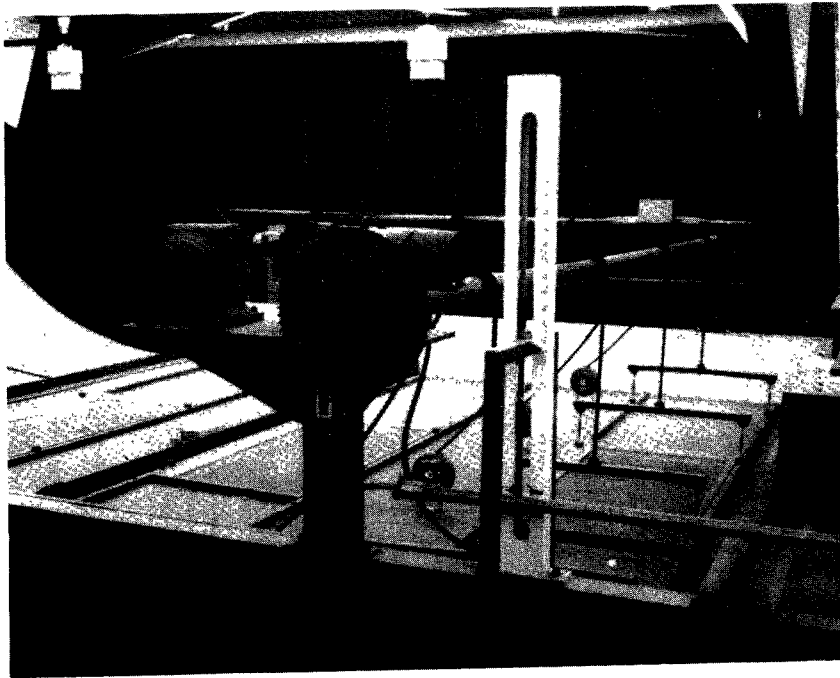


Figure 12. Gear motor, limit switches, and torque tube.

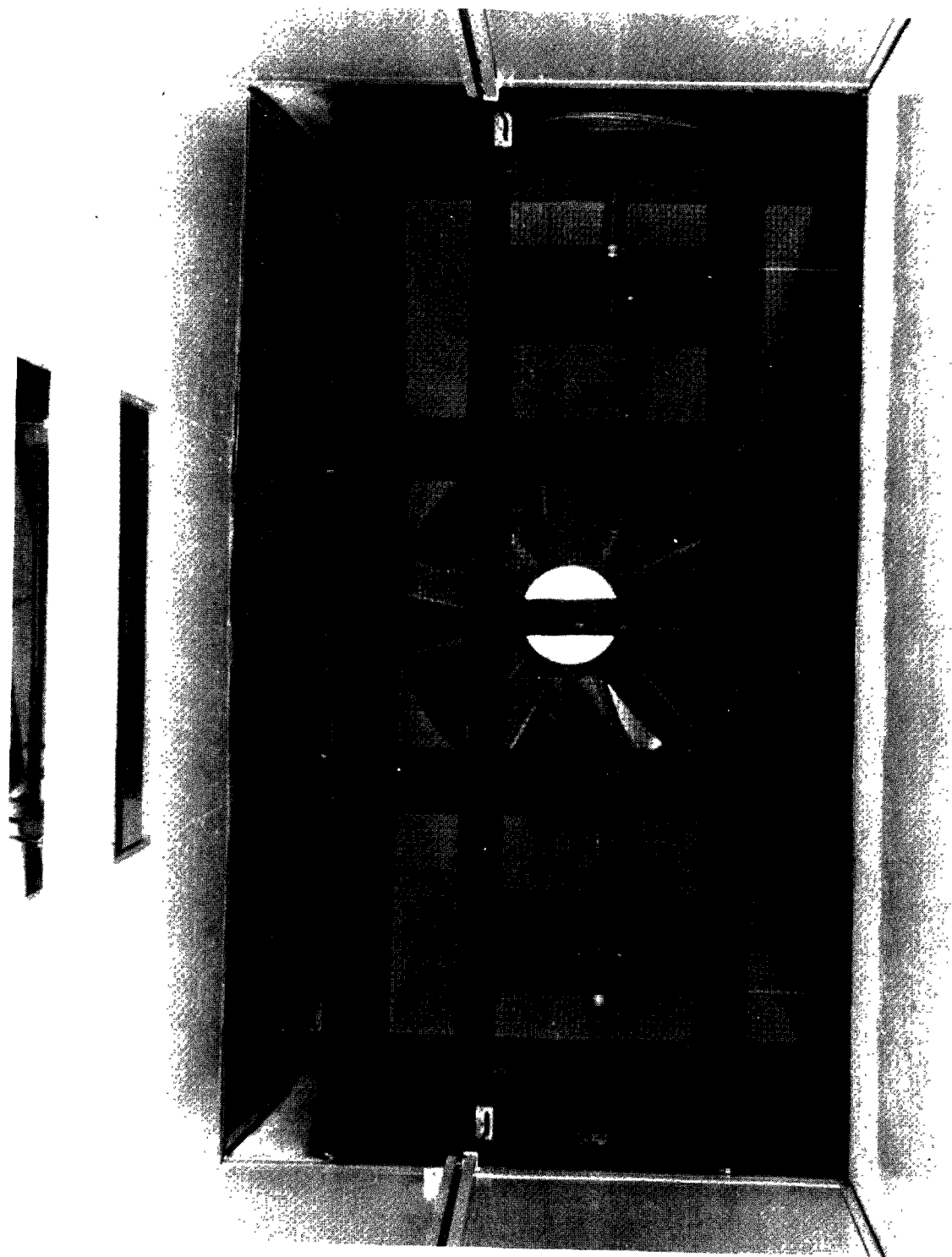


Figure 13. Inlet silencer.

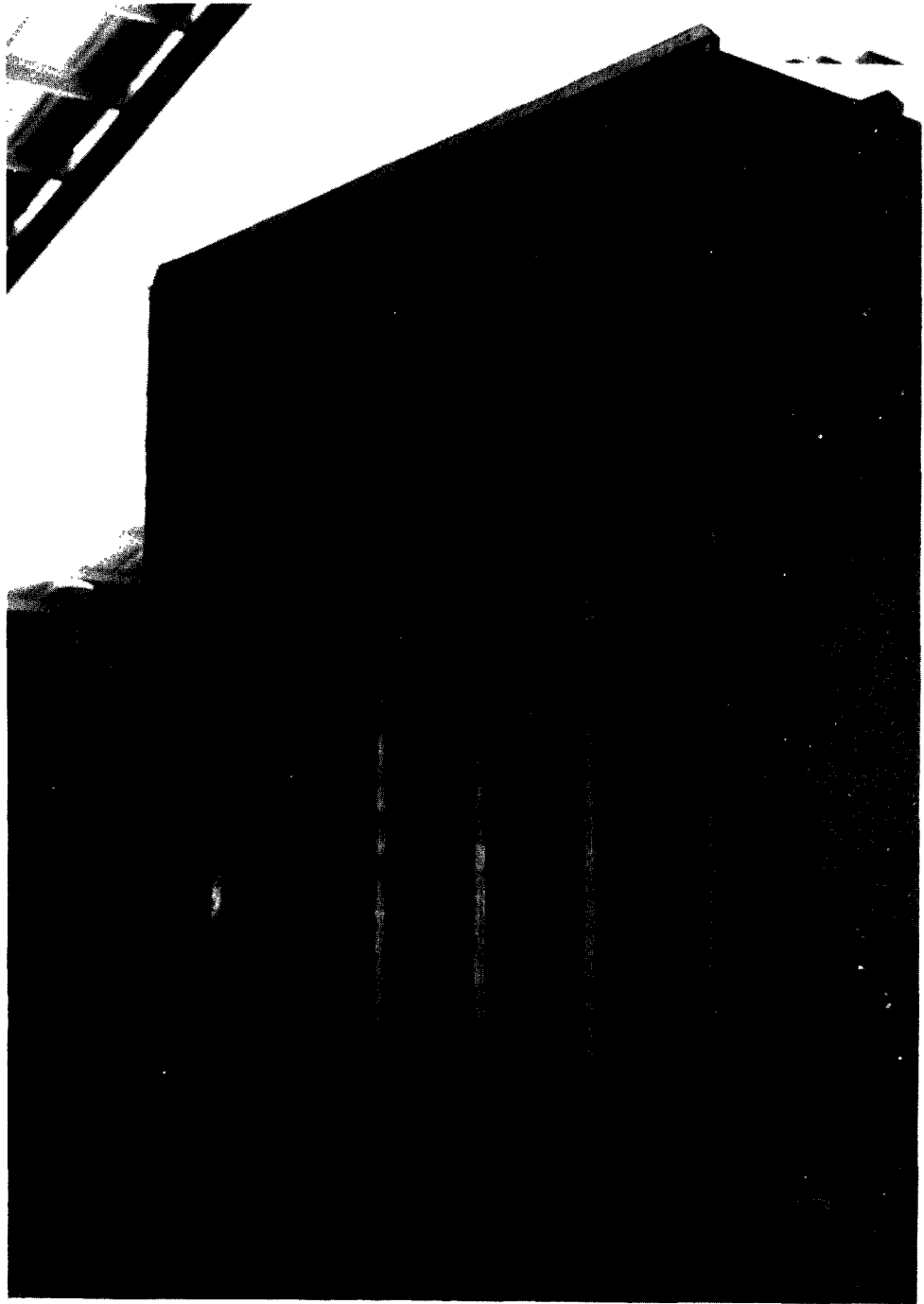


Figure 14. Exhaust silencer.

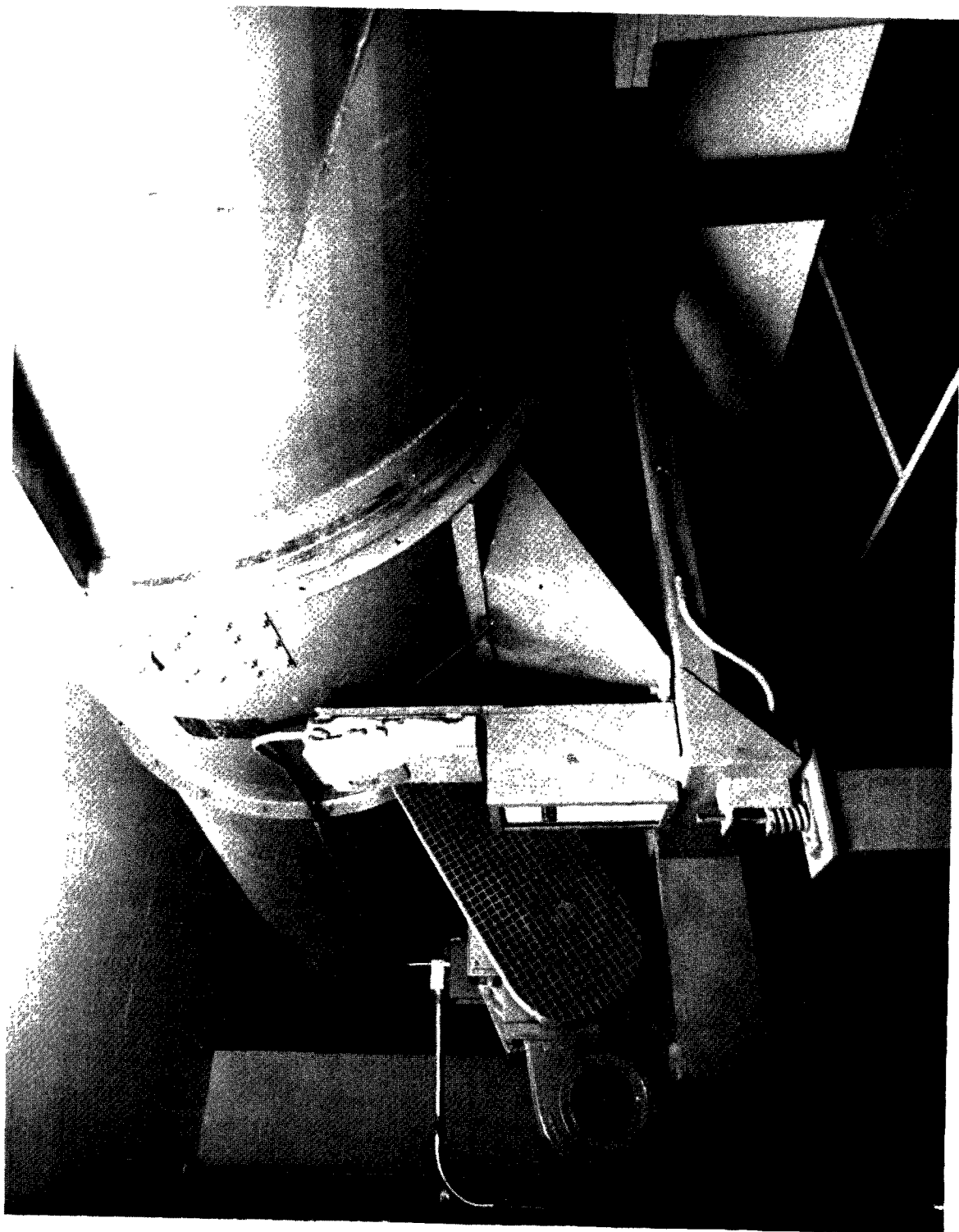


Figure 15. View of fan and motor from inside sound enclosure.

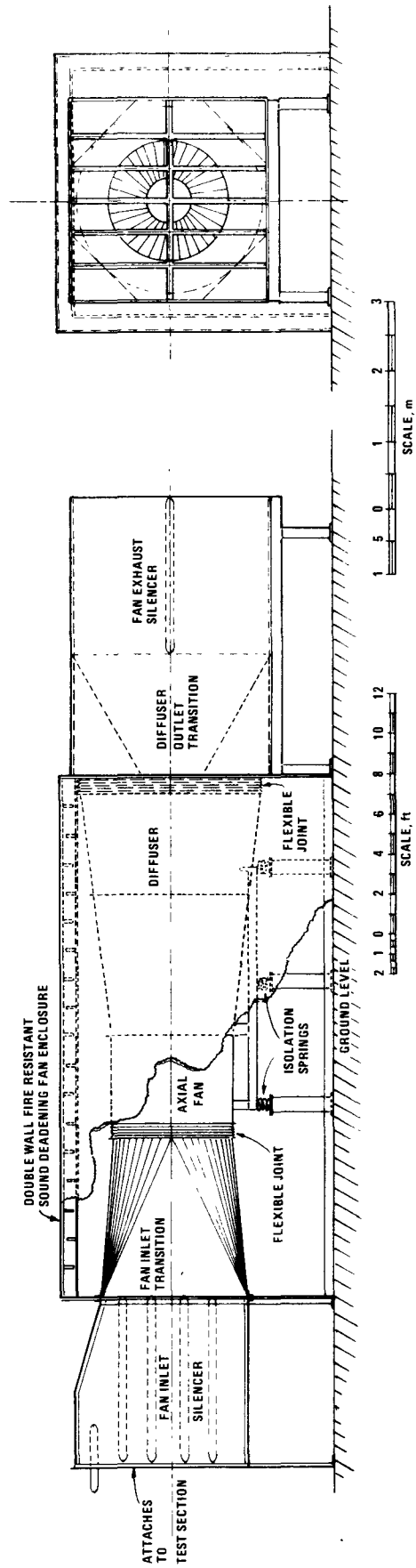


Figure 16. Tail section assembly.

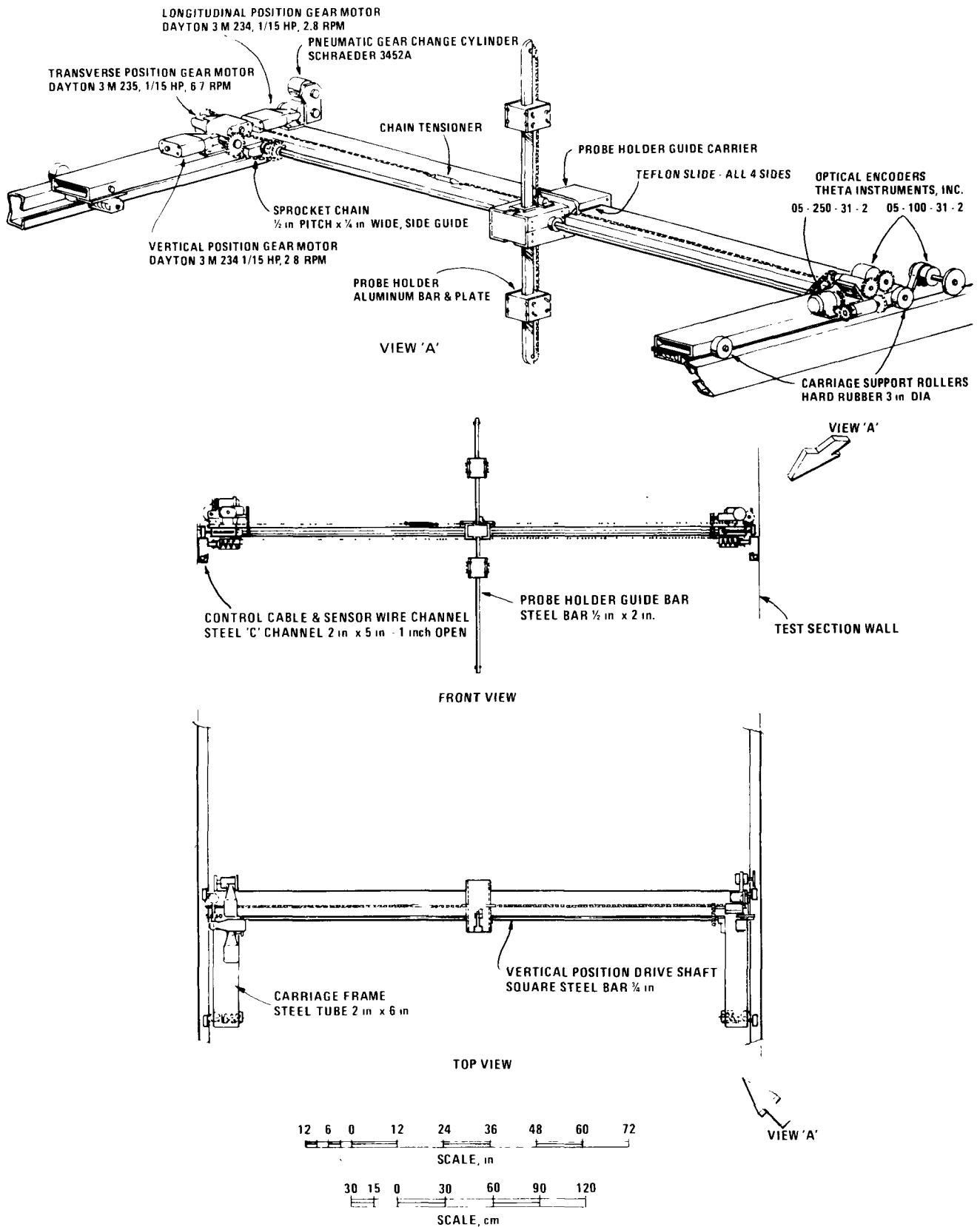
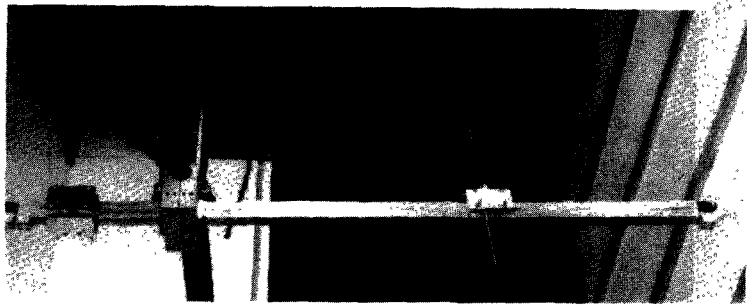


Figure 17. Instrument carriage.



MOTOR DRIVES
(LEFT SIDE)



VERTICAL BAR
(CENTER)



OPTICAL ENCODERS
(RIGHT SIDE)

Figure 18. Views of instrument carriage.



Figure 19. Close-up view of cable drum.

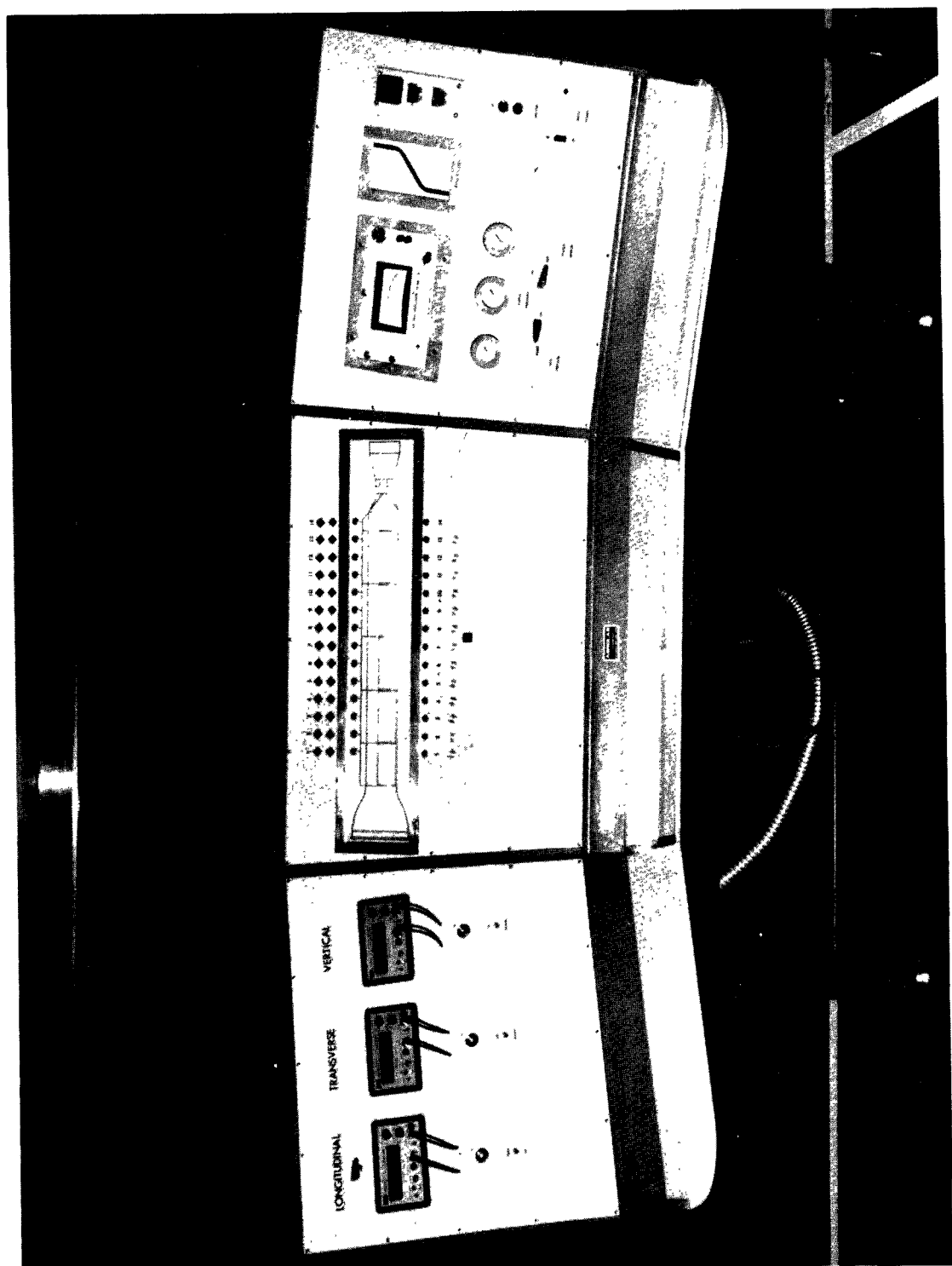


Figure 20. Operators' Console.

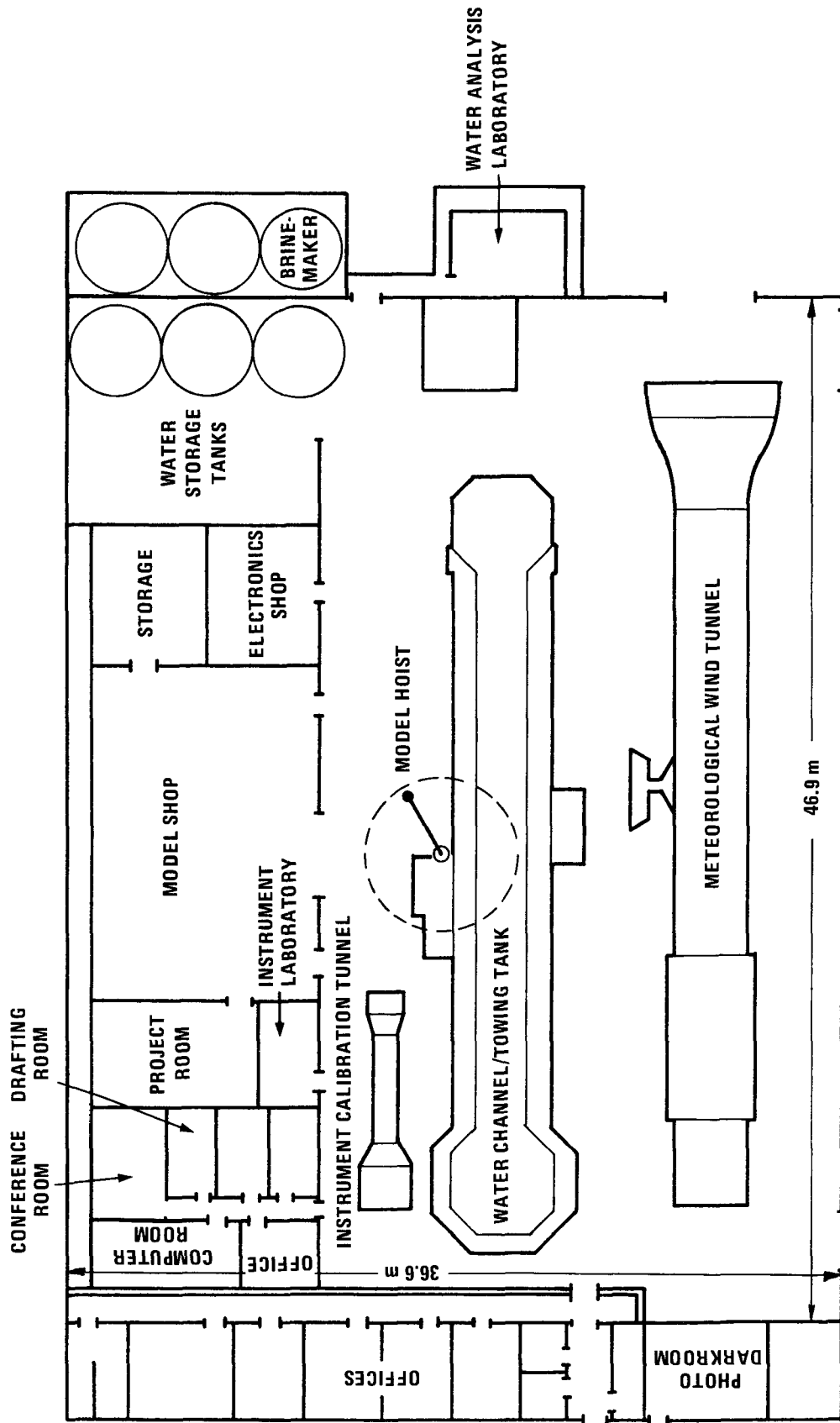


Figure 21. Floor plan of Fluid Modeling Facility.

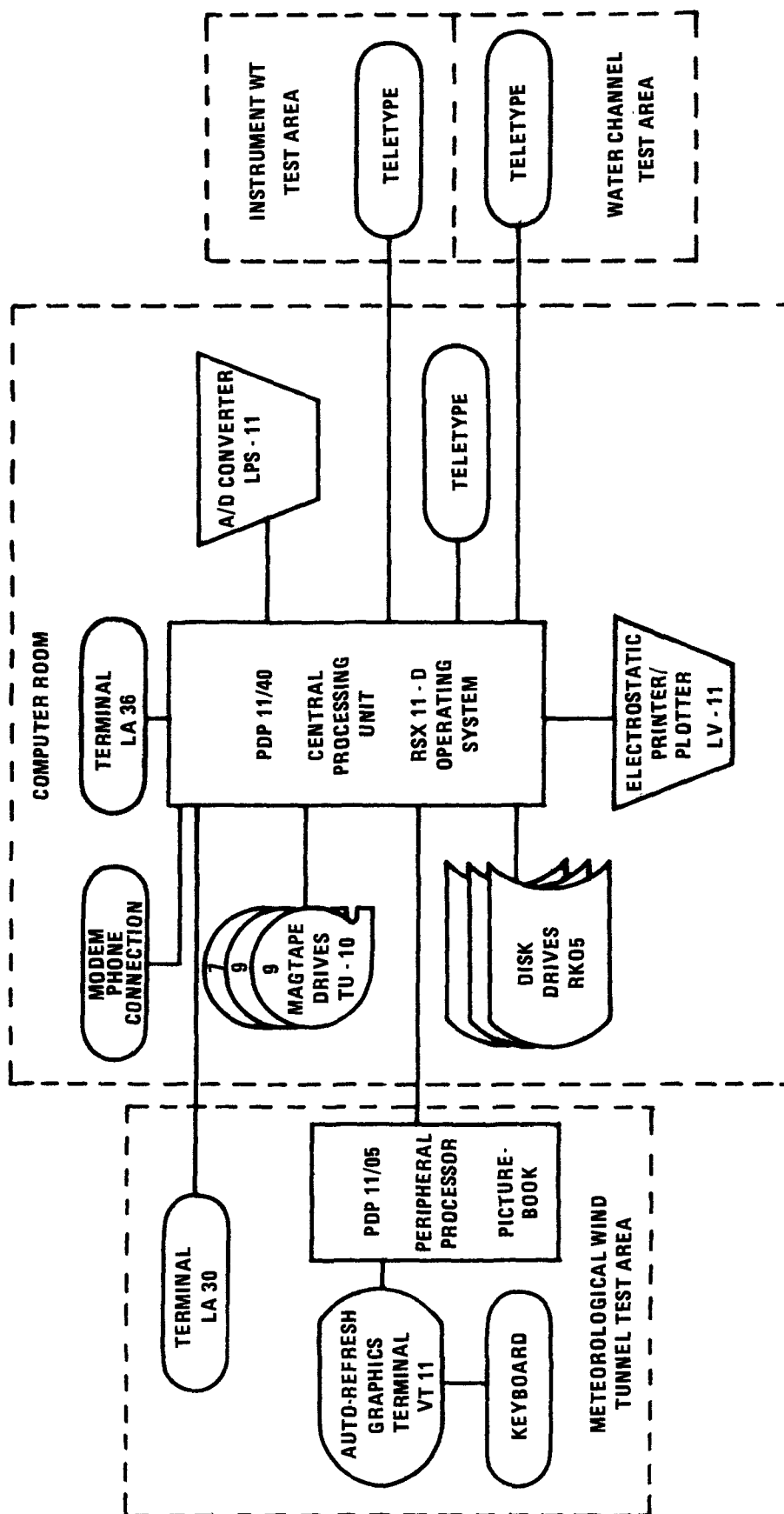


Figure 22. Schematic of minicomputer system.

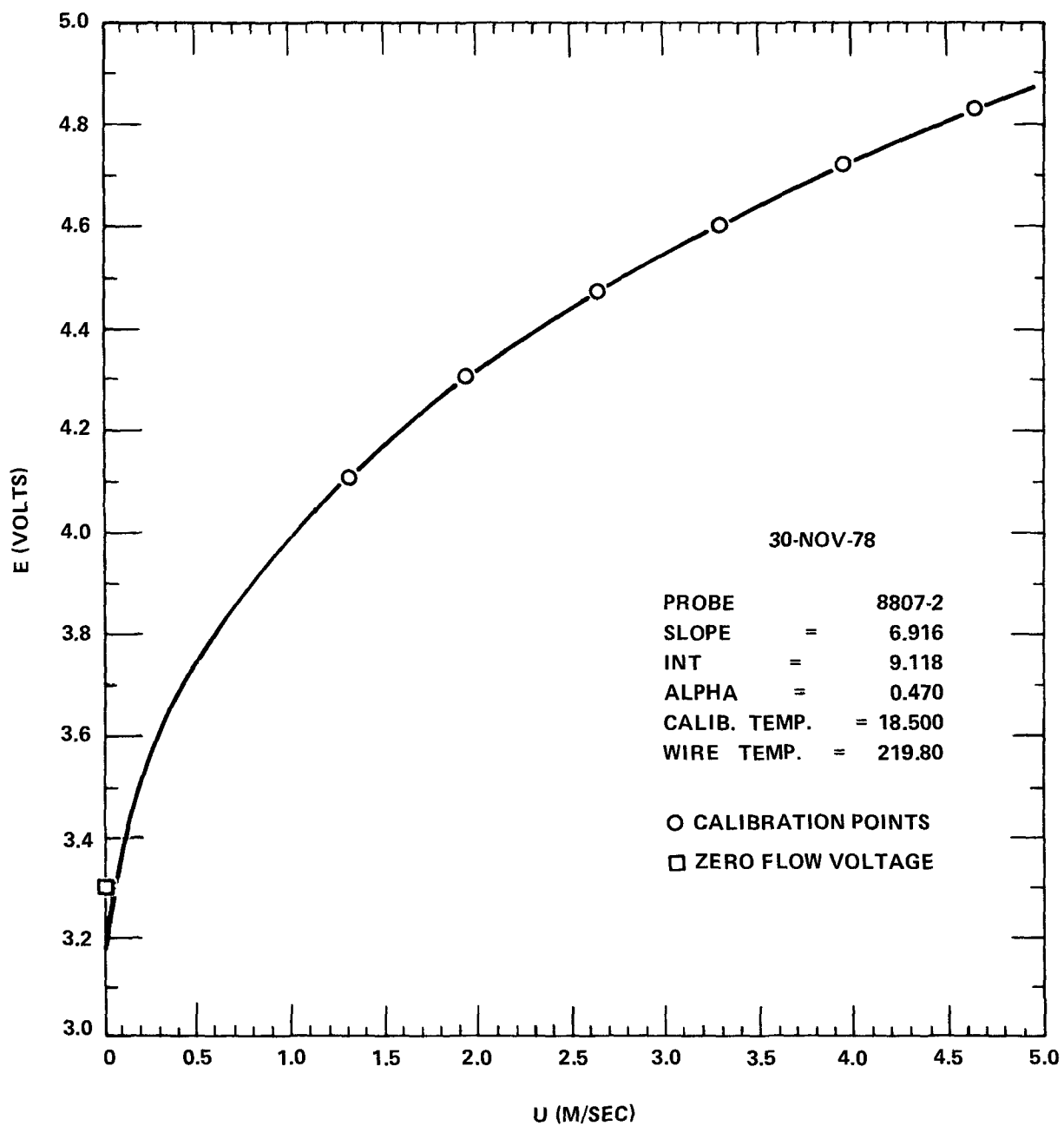


Figure 23. Typical calibration curve for hot-film probe.

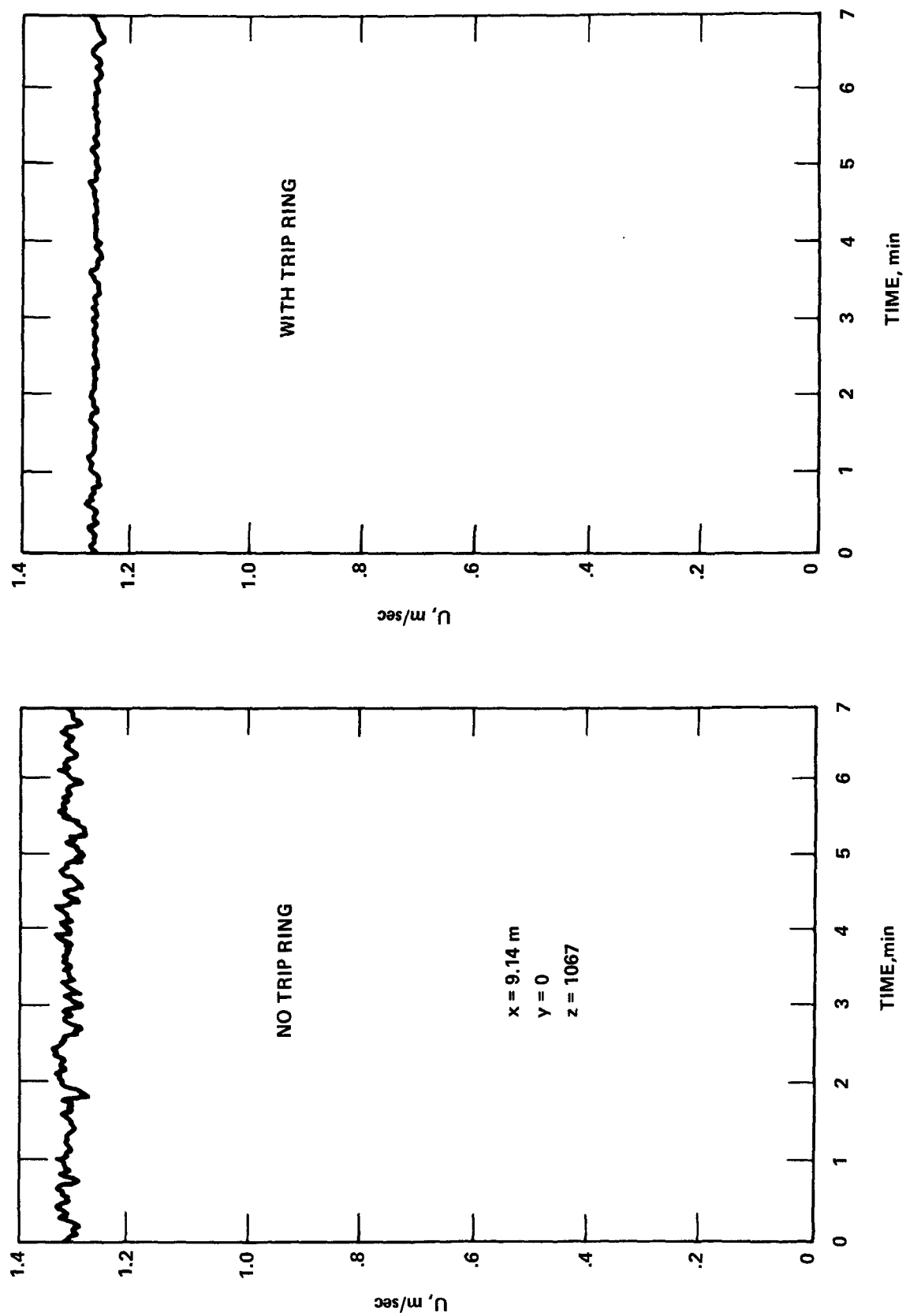


Figure 24. Effect of trip ring on velocity and velocity fluctuations.

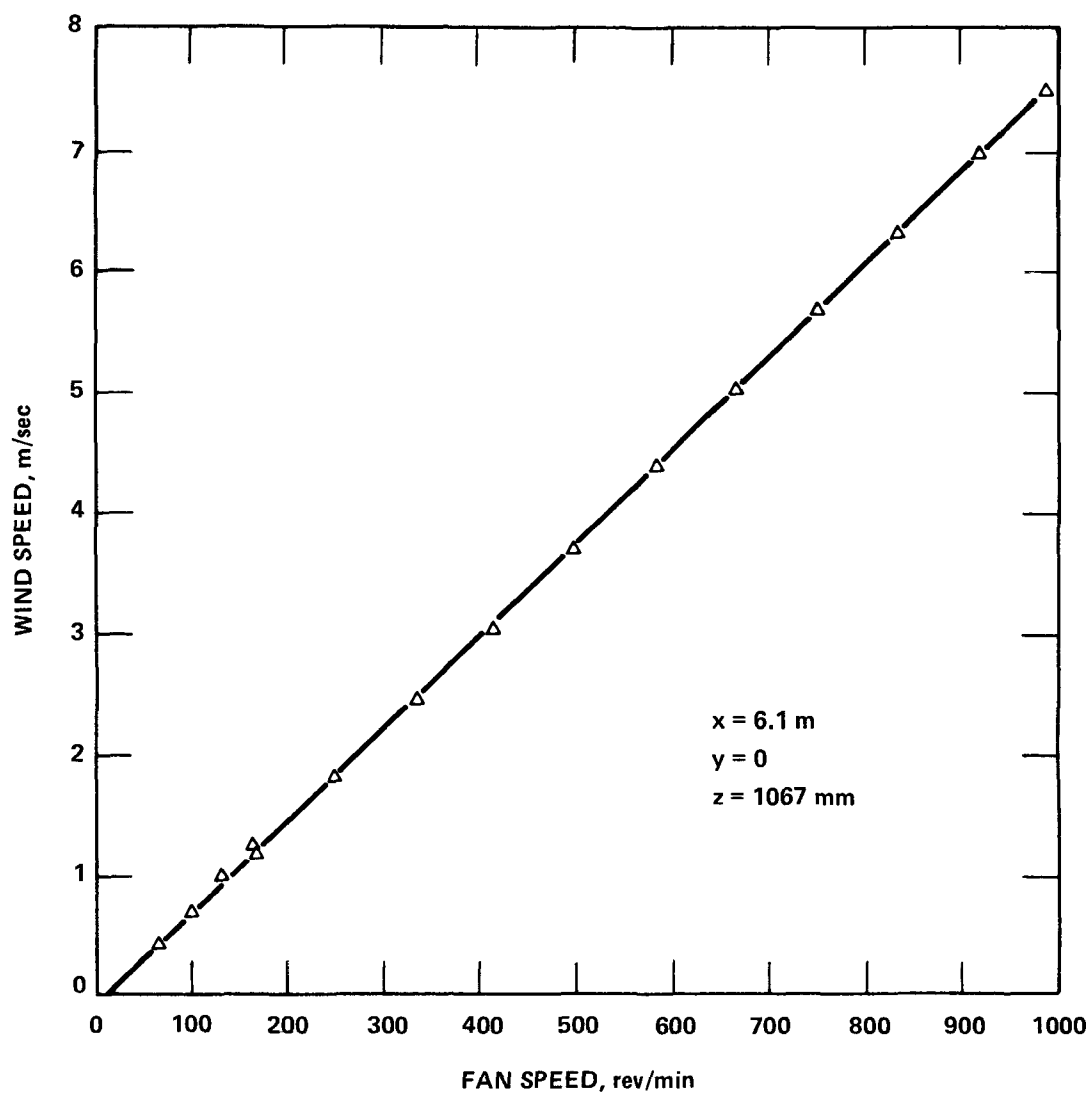


Figure 25. Calibration of empty wind tunnel; air speed as a function of fan speed.

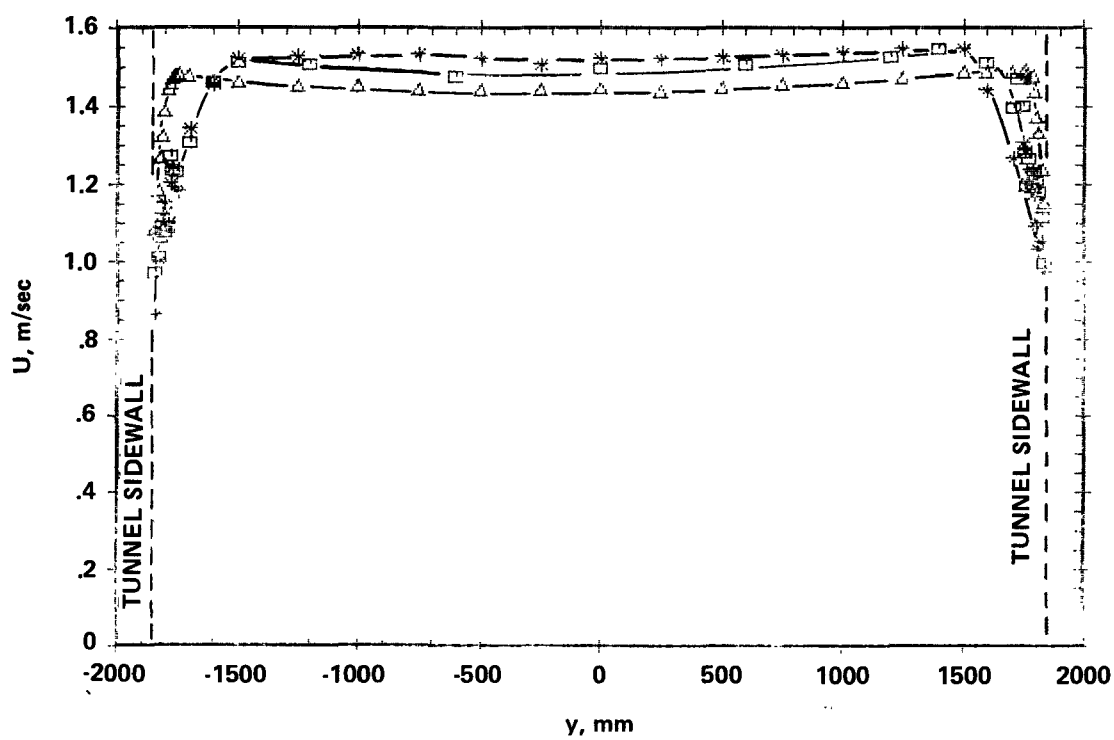
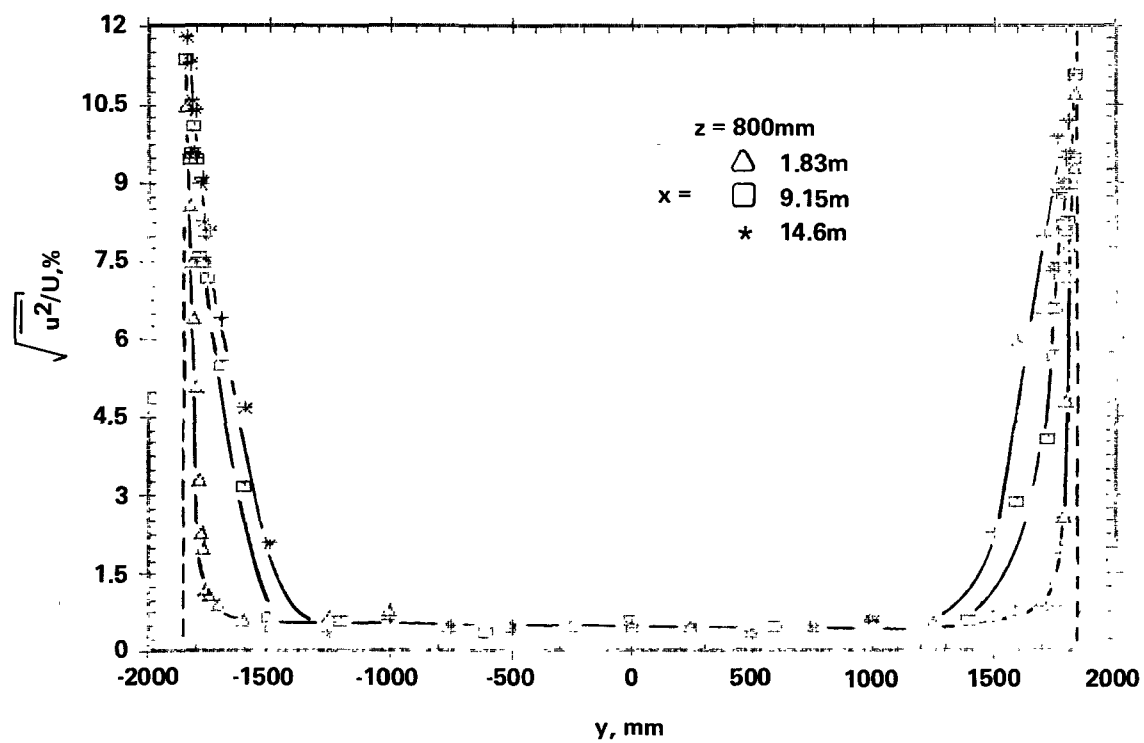


Figure 26. Lateral mean velocity and turbulence intensity profiles; $U = 1.5\text{m/sec}$.

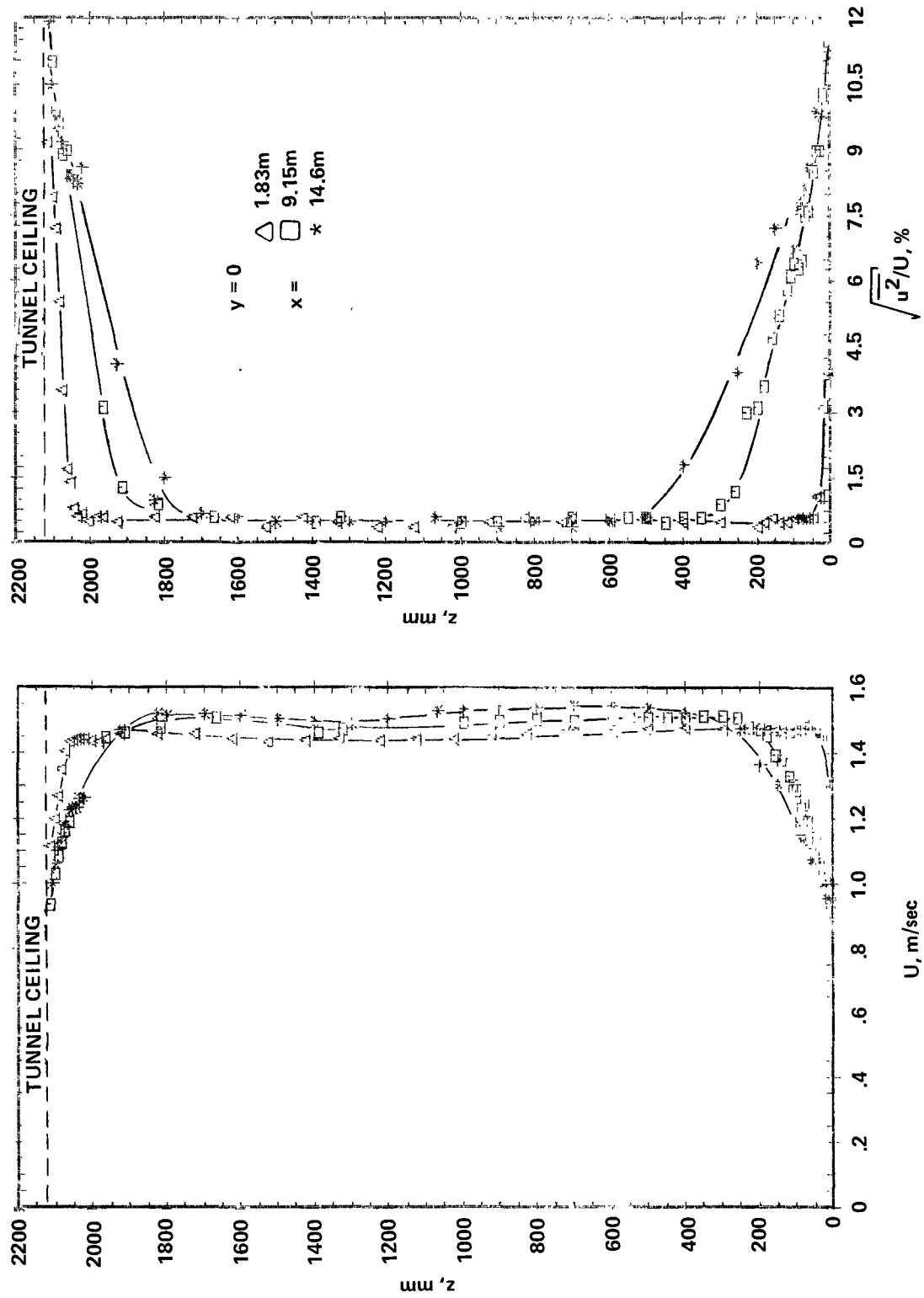


Figure 27. Vertical mean velocity and turbulence intensity profiles; $U = 1.5$ m/sec.

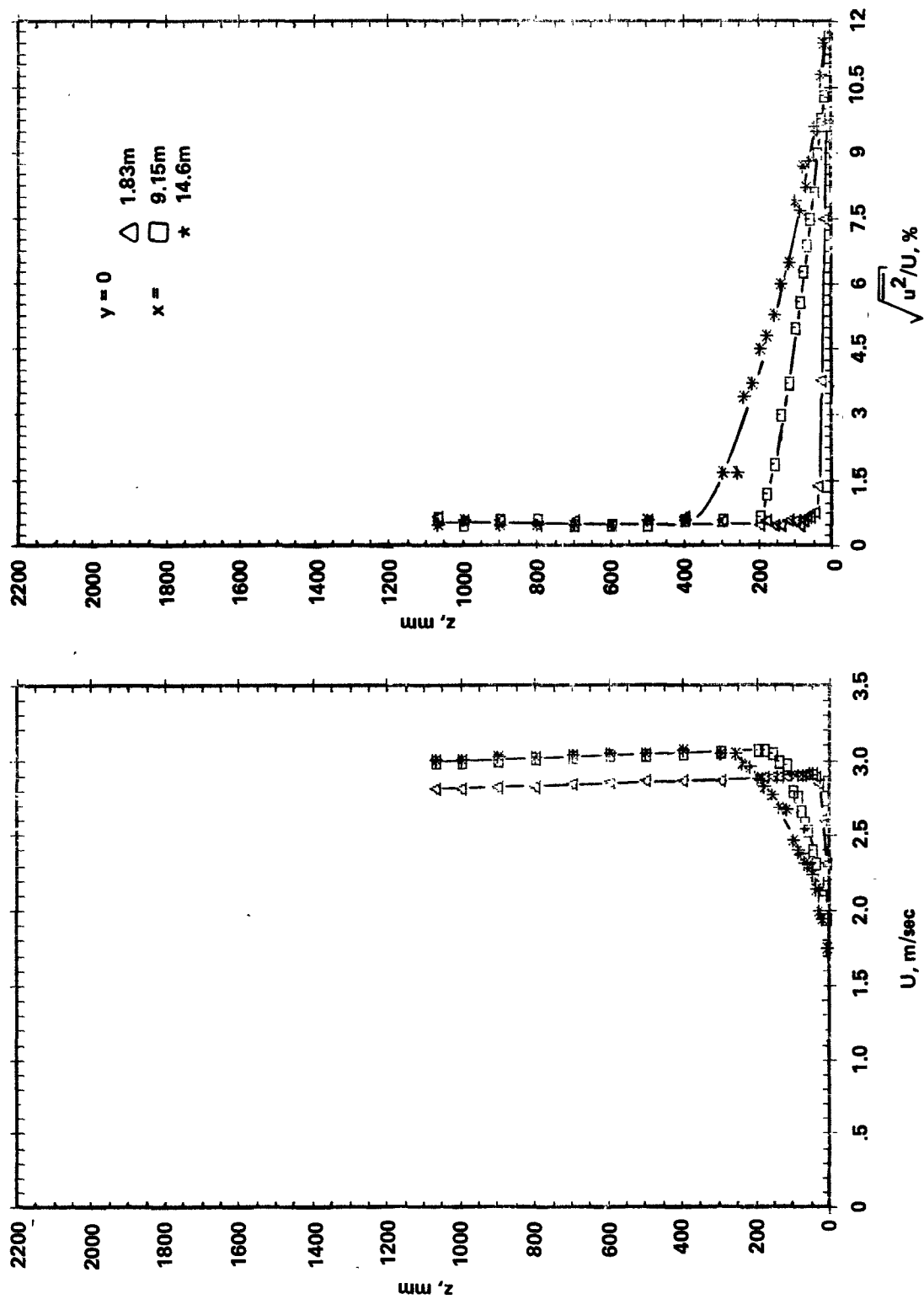


Figure 28. Vertical mean velocity and turbulence intensity profiles; $U = 3\text{m/sec}$.

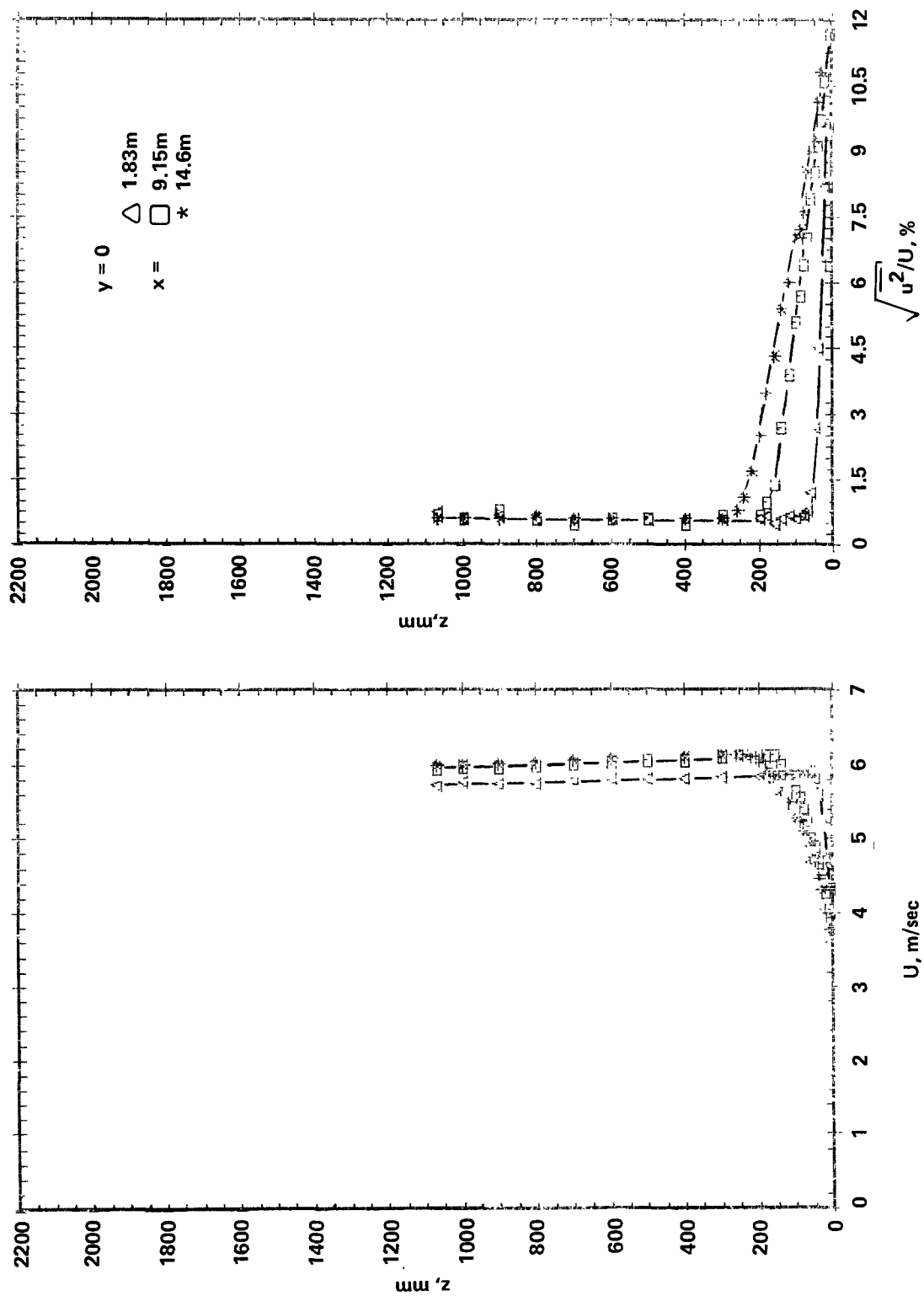


Figure 29. Vertical mean velocity and turbulence intensity profiles; $U = 6\text{m/sec}$.

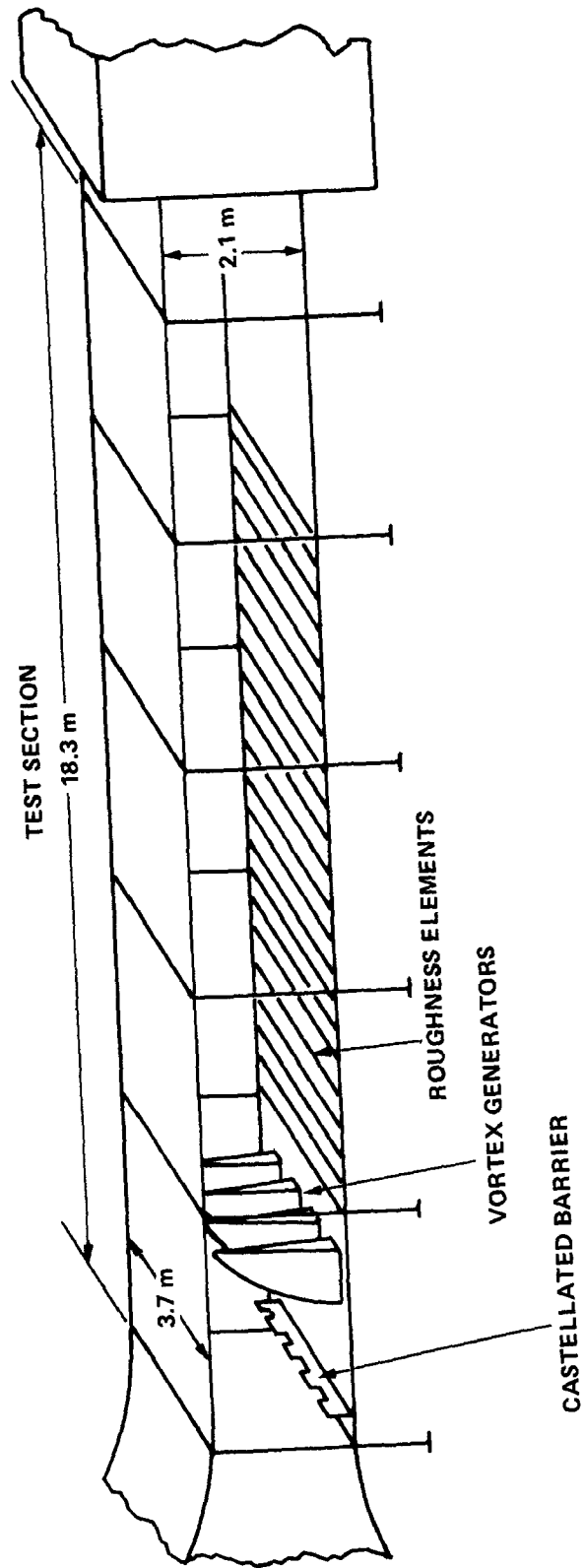


Figure 30. Vortex generator system.

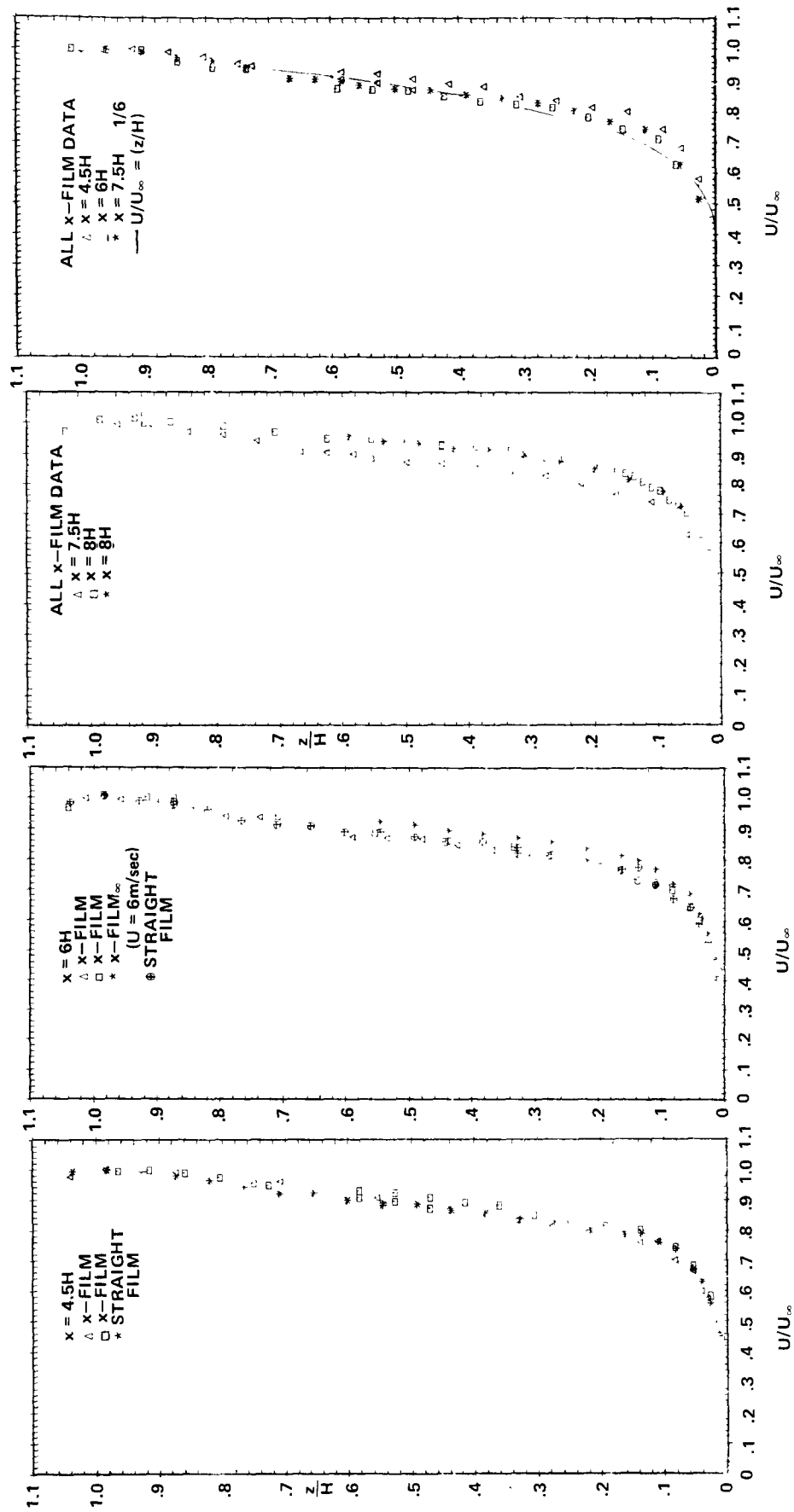


Figure 31. Development of mean velocity profile along centerline of wind tunnel; $U_\infty = 3 \text{ m/s}$ (except as noted).

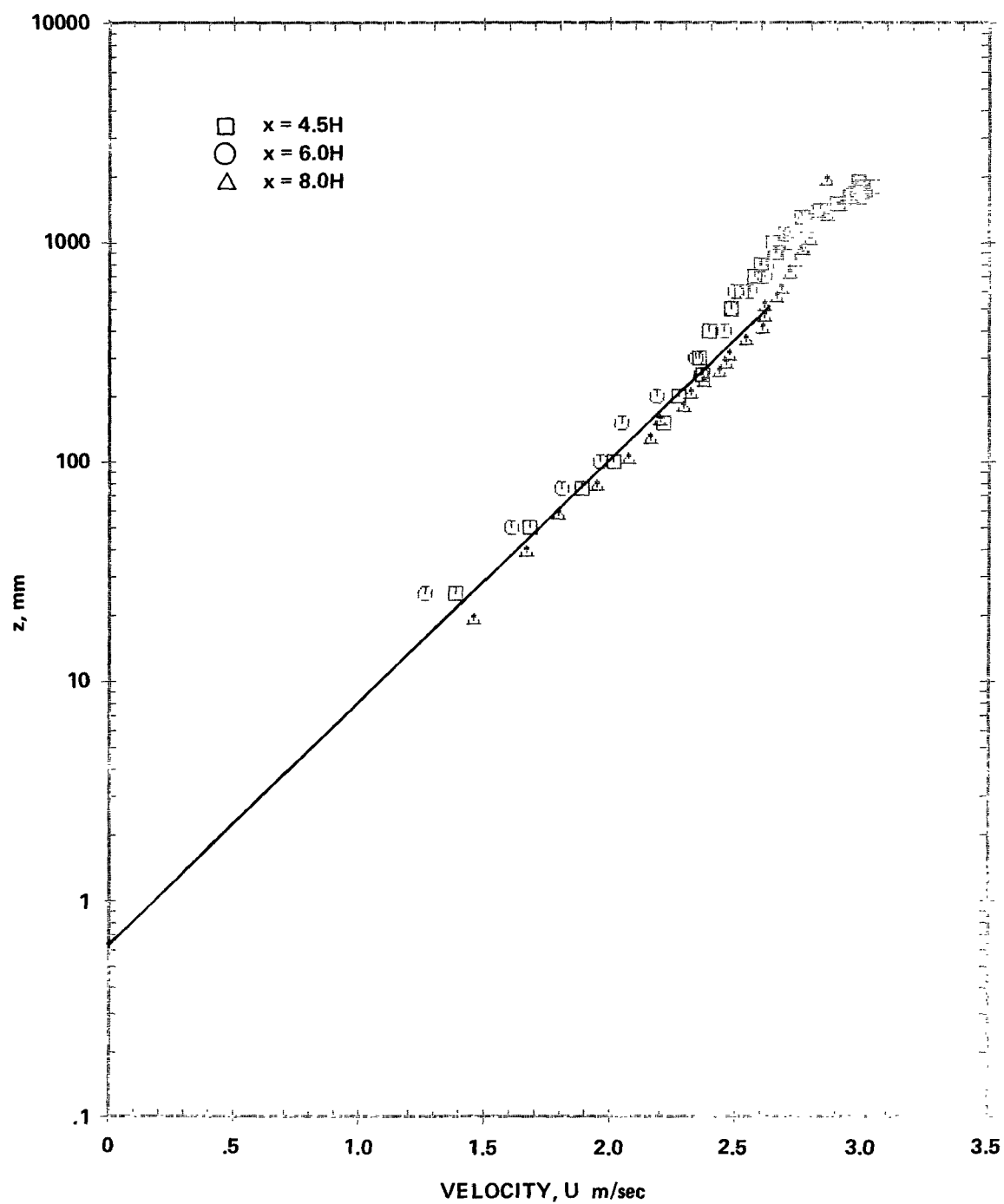


Figure 32. Mean velocity profiles in log-law form.

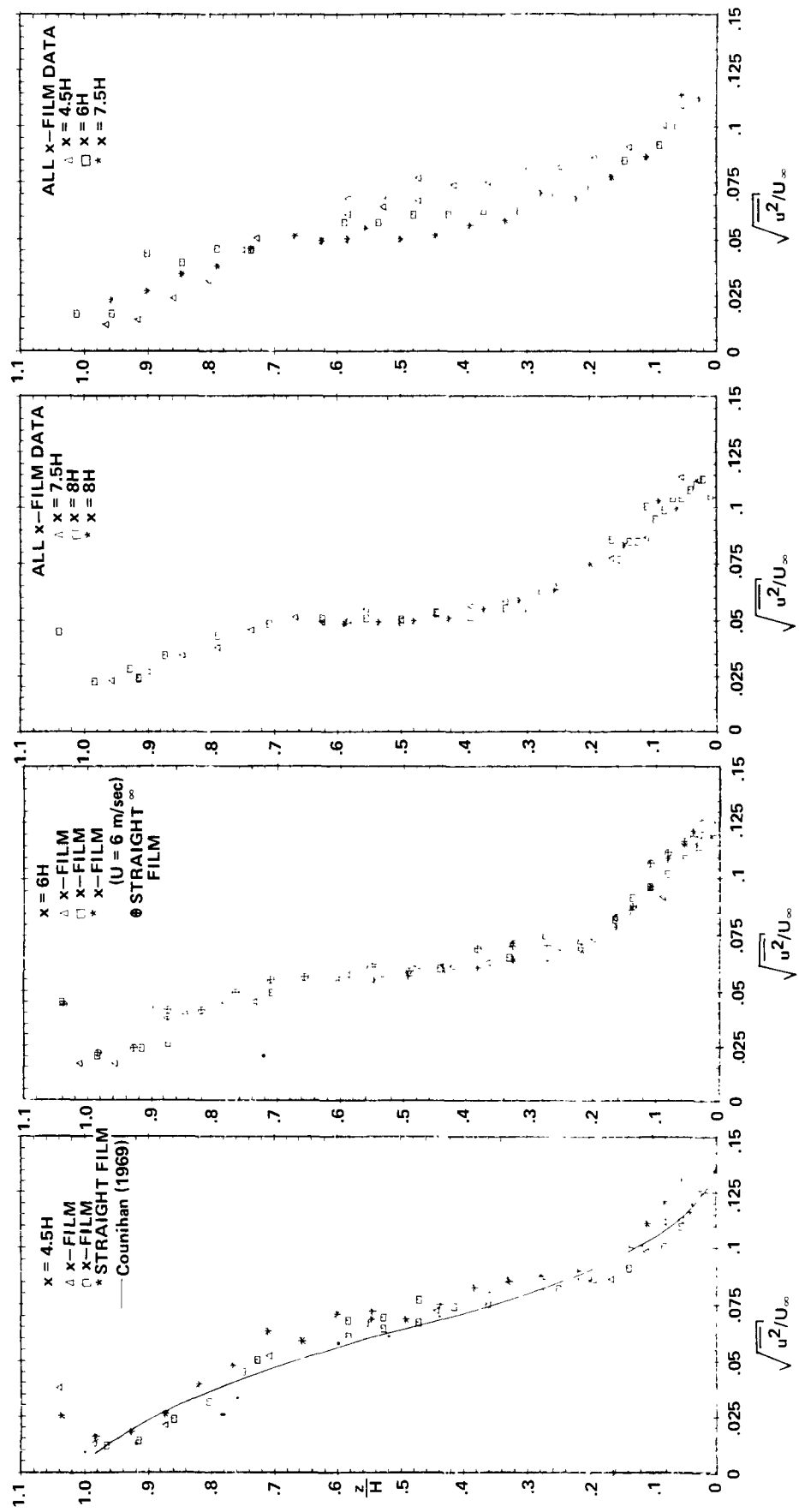


Figure 33. Development of longitudinal turbulence intensity along centerline of wind tunnel; $U_\infty = 3\text{m/s}$ (except as noted).

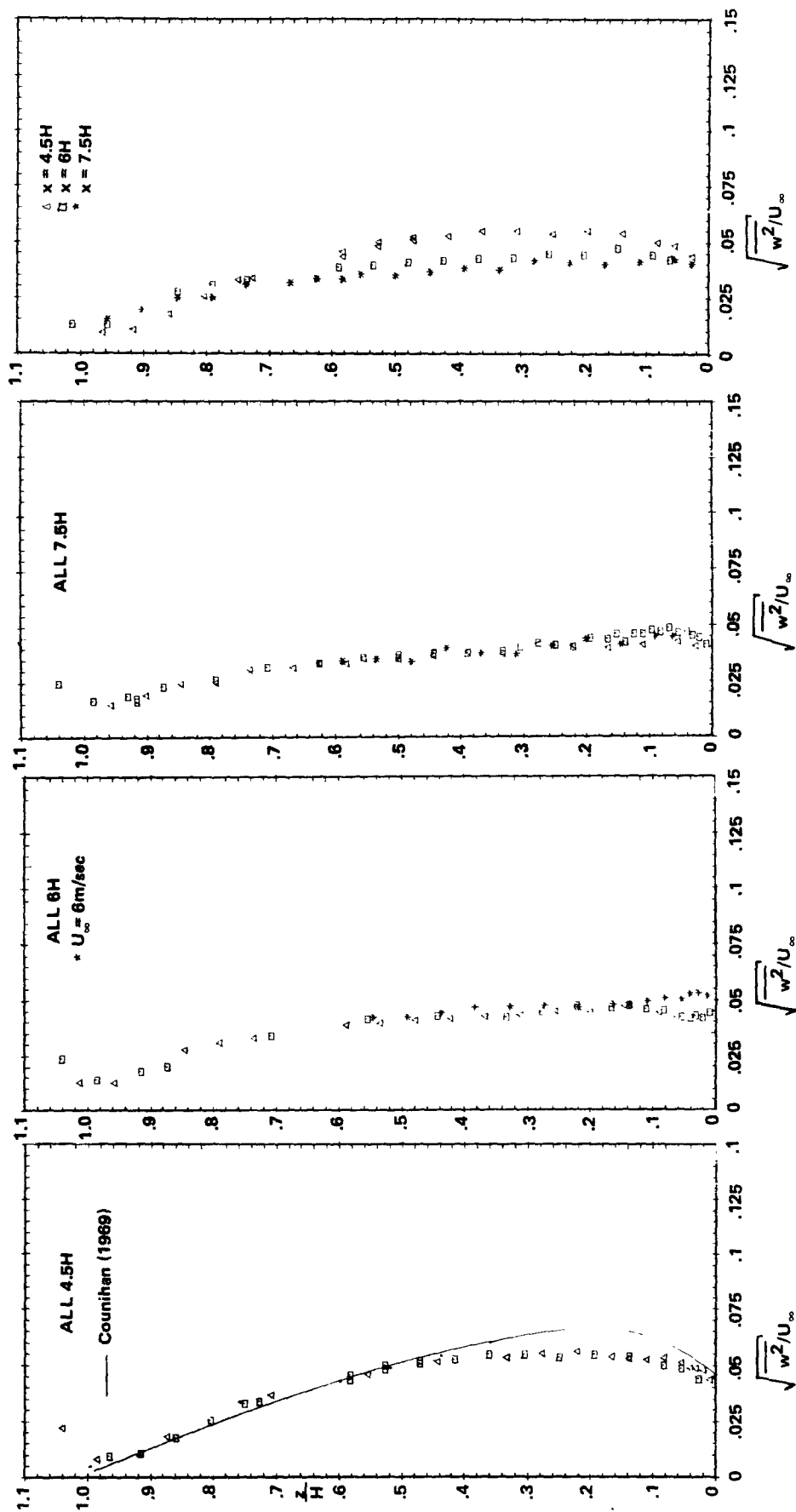


Figure 34. Development of vertical turbulence intensity along centerline of wind tunnel; $U_\infty = 3\text{m/s}$ (except as noted).

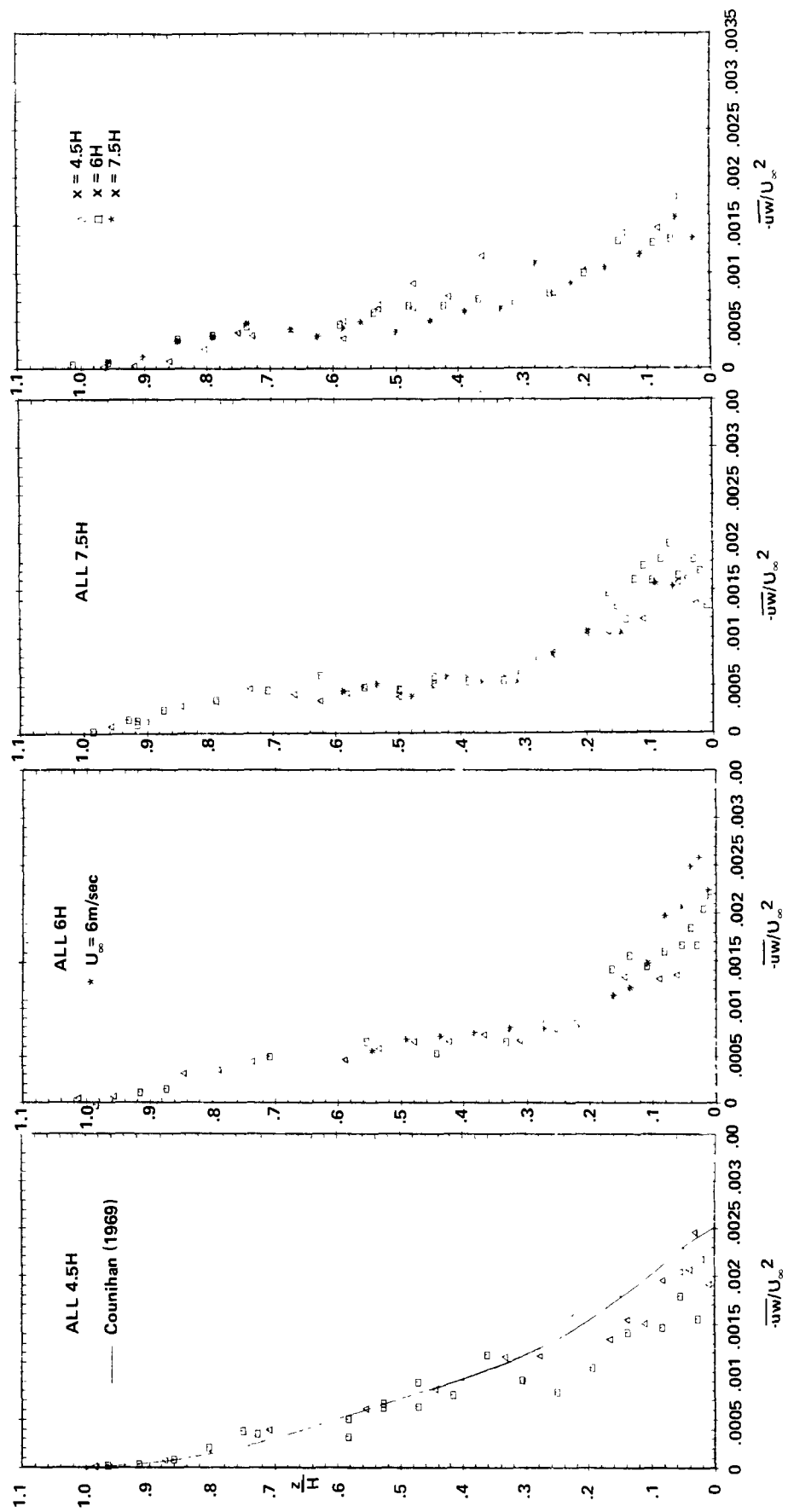


Figure 35. Development of Reynolds stress along centerline of wind tunnel; $U = 3\text{m/s}$ (except as noted).

	x/H	z/H
△	4.5	.083
□	6.0	
*	7.5	
⊕	4.5	.333
⊗	6.0	
+	7.5	
×	4.5	.833
⋈	6.0	
#	7.5	

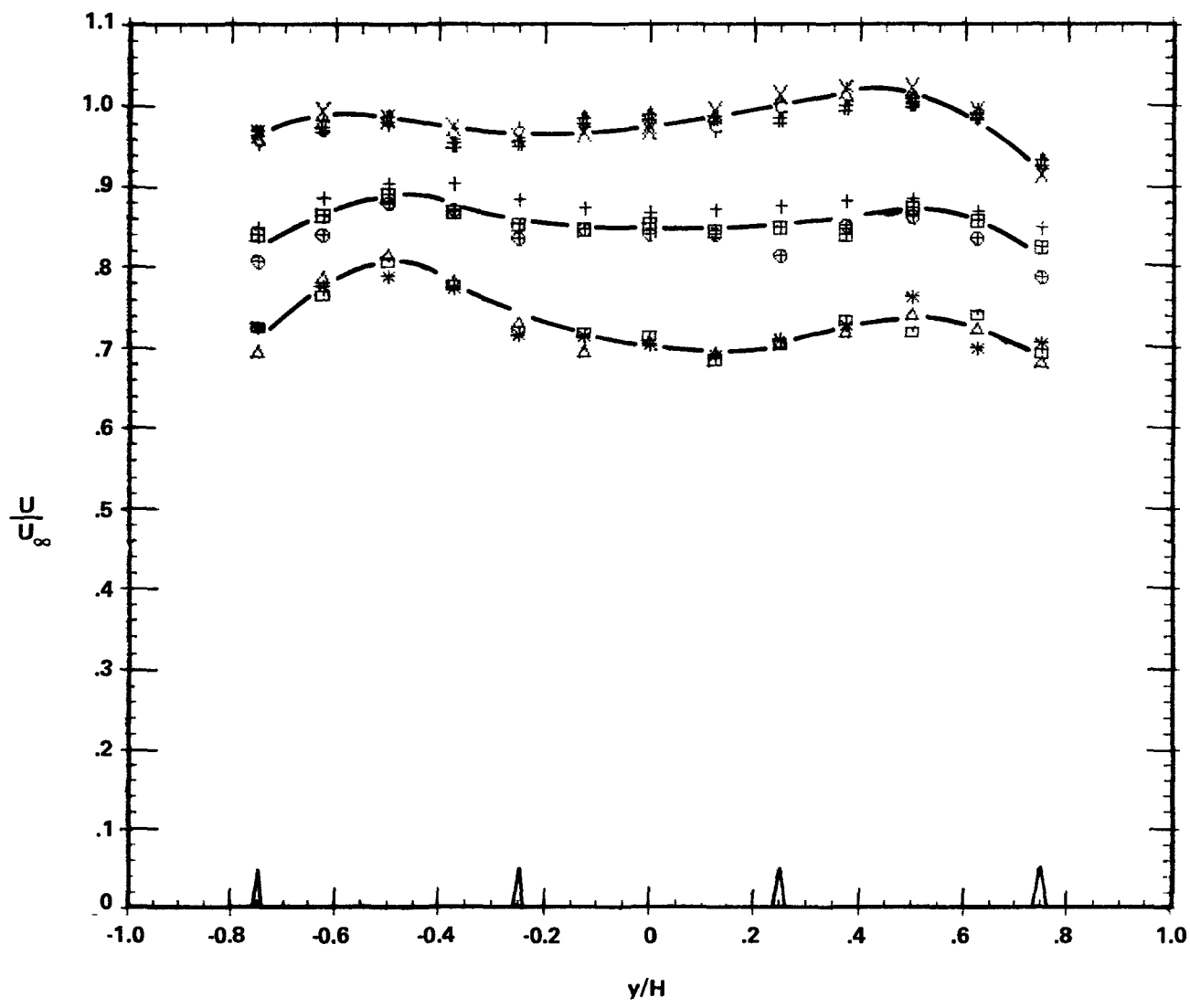


Figure 36. Lateral uniformity of mean velocity; $U_\infty=3\text{m/s}$.

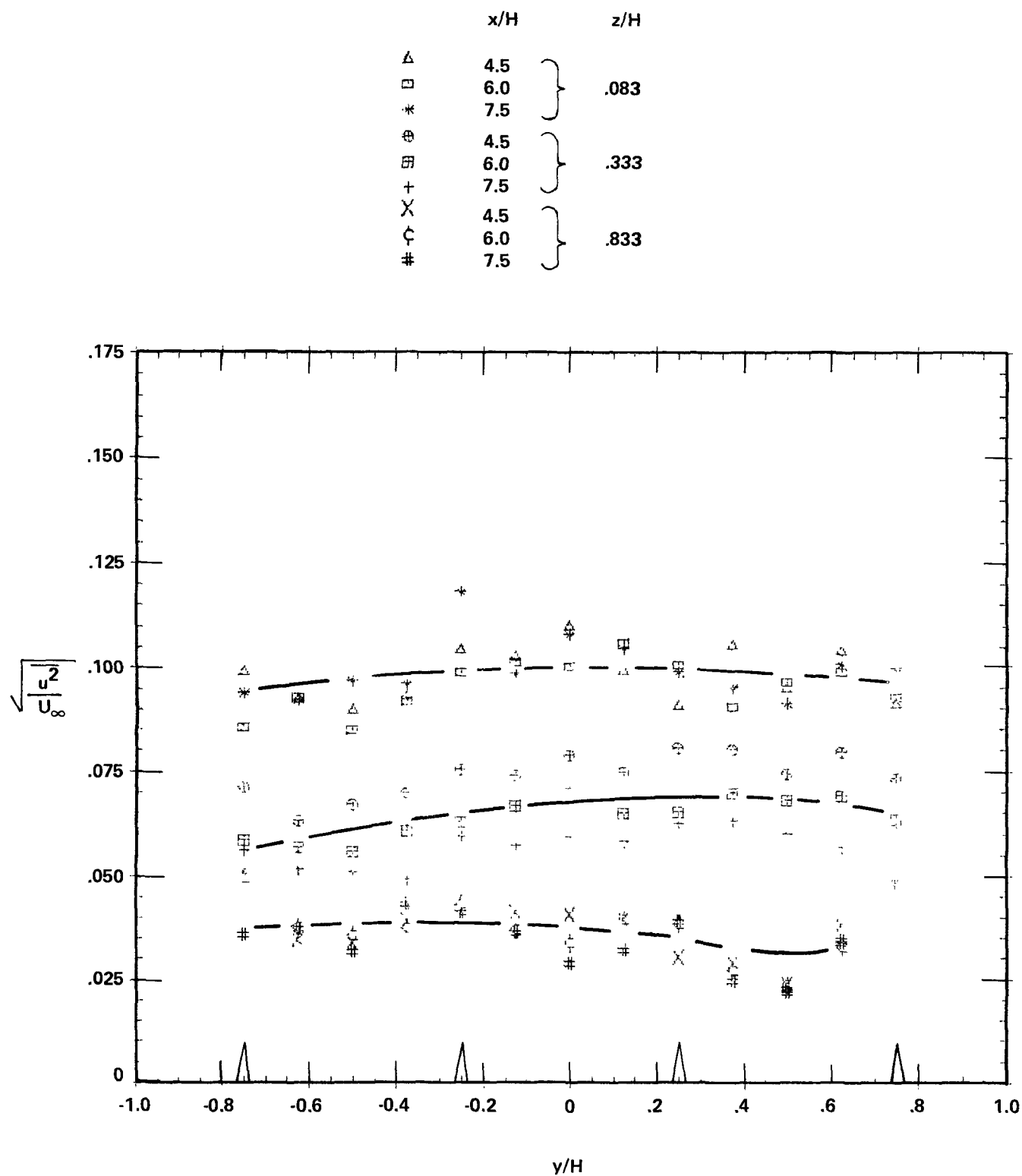


Figure 37. Lateral uniformity of longitudinal turbulence intensity; $U_{\infty} = 3\text{m/s}$.

	x/H		z/H
△	4.5	}	.083
□	6.0		
*	7.5		
⊕	4.5	}	.333
⊗	6.0		
+	7.5		
×	4.5	}	.833
⋈	6.0		
#	7.5		

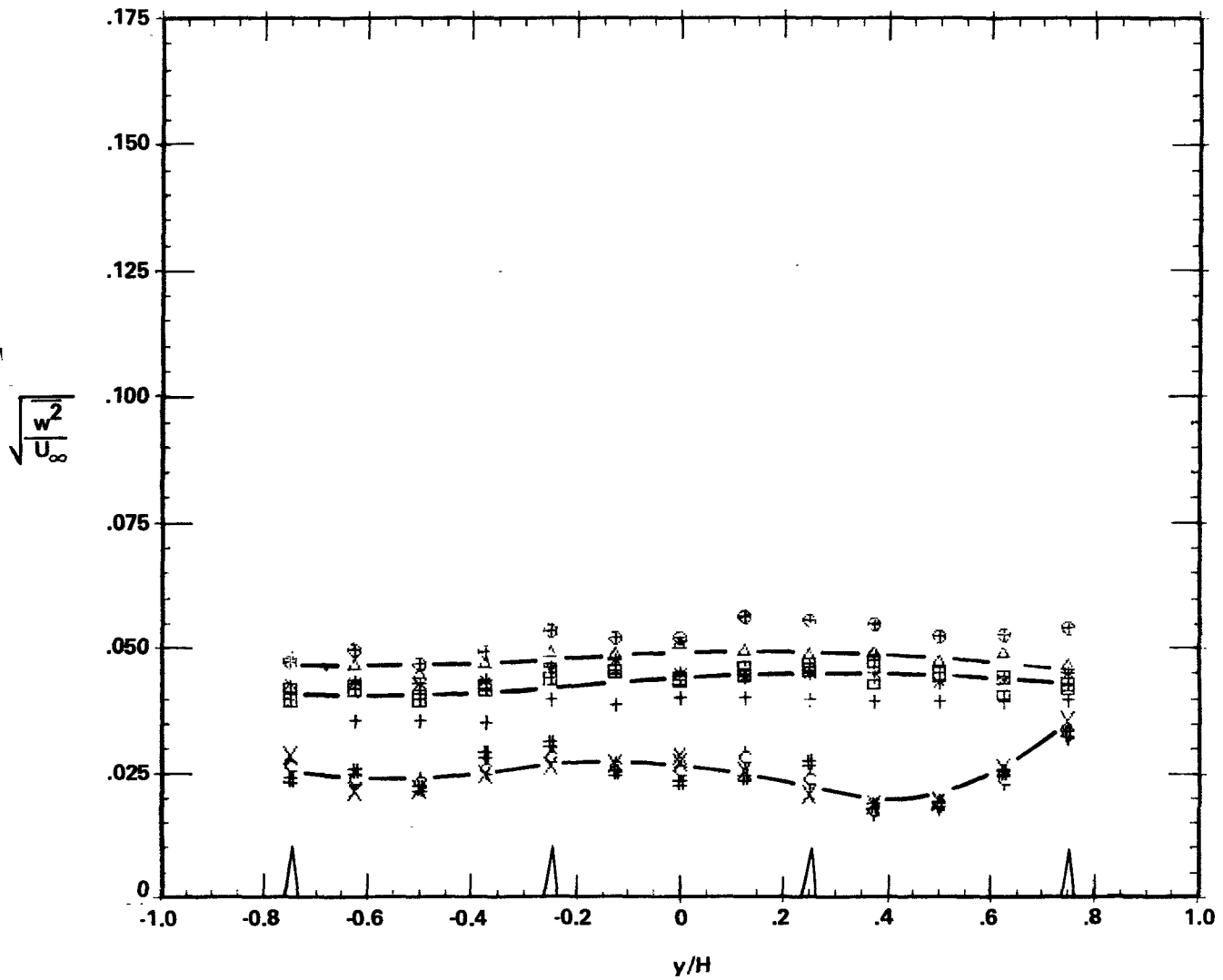


Figure 38. Lateral uniformity of vertical turbulence intensity; $U_\infty = 3\text{m/s}$.

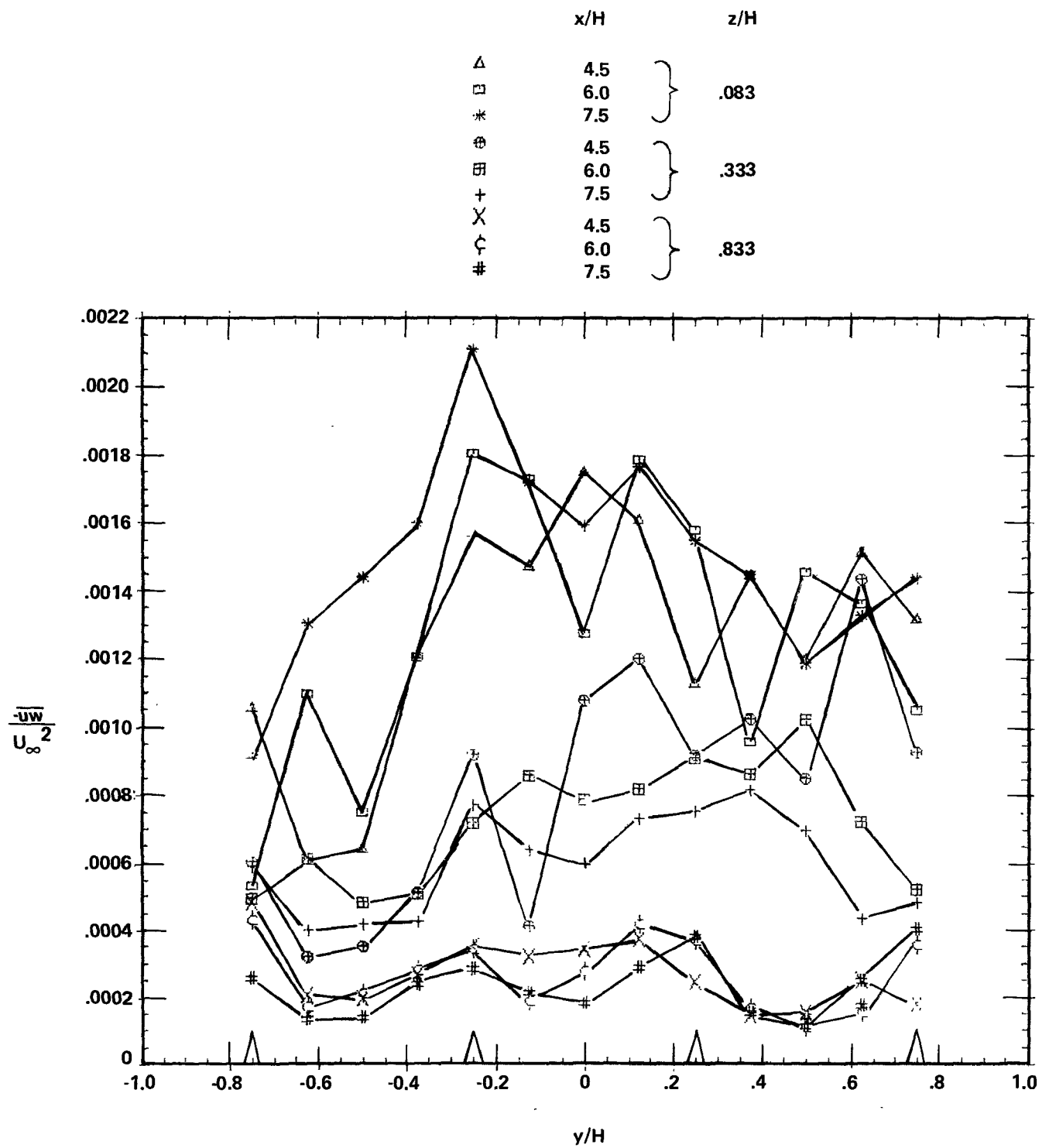


Figure 39. Lateral uniformity of Reynolds stress; $U_{\infty} = 3\text{m/s}$.

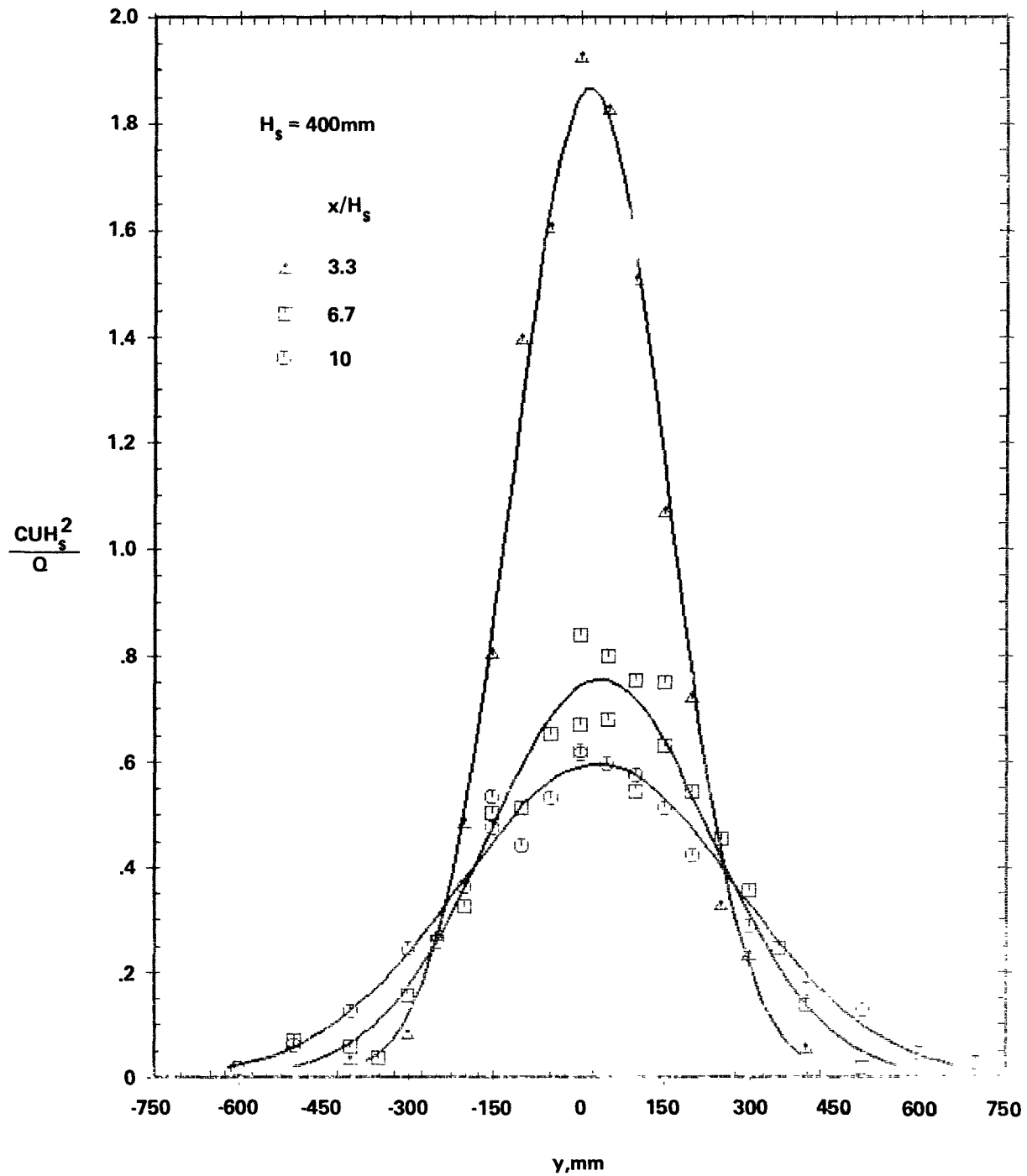


Figure 40. Lateral concentration profiles taken through plume centerline; $U_\infty = 3\text{m/s}$.

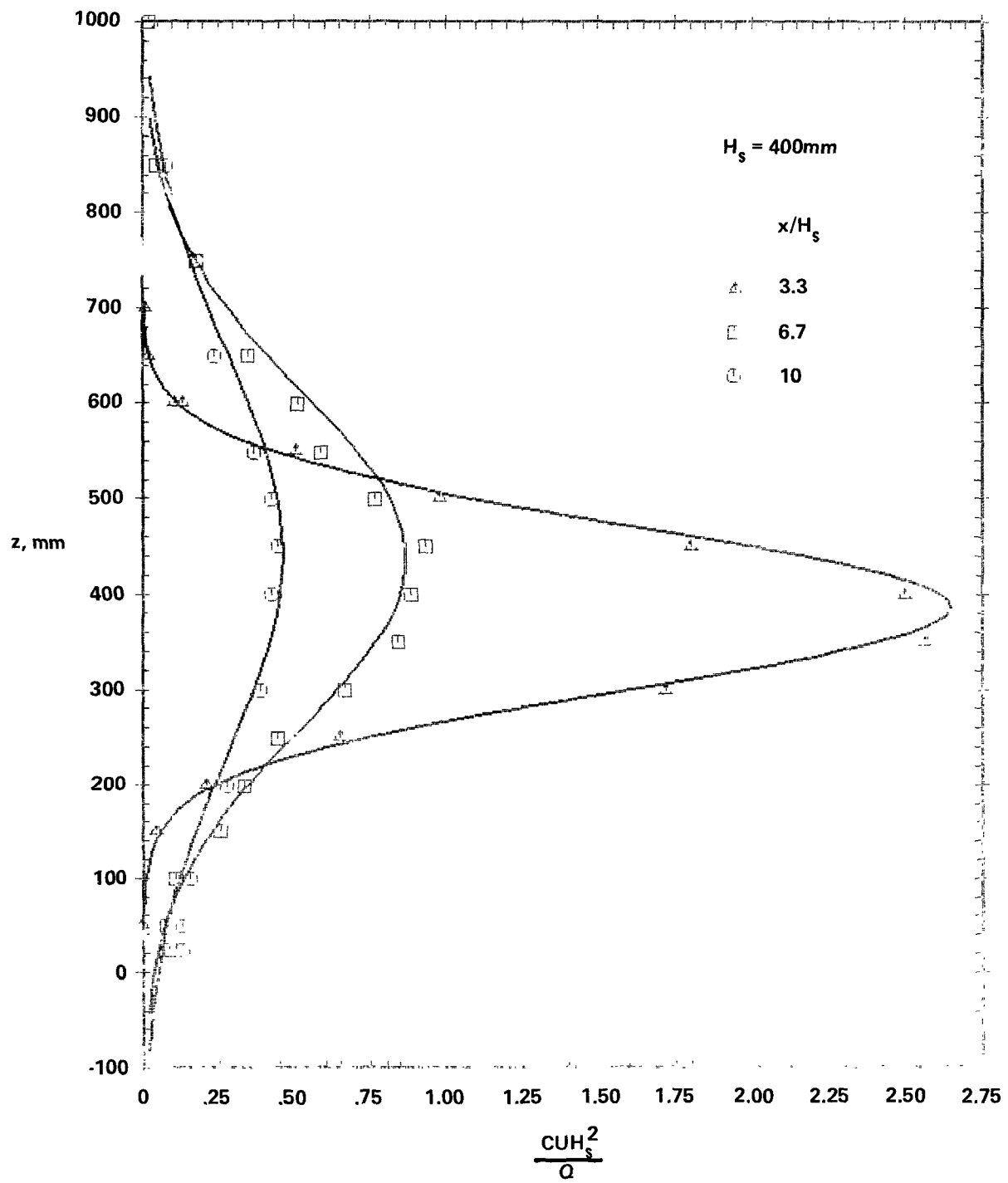


Figure 41. Vertical concentration profiles taken through plume centerline; $U_\infty = 3\text{m/s}$.

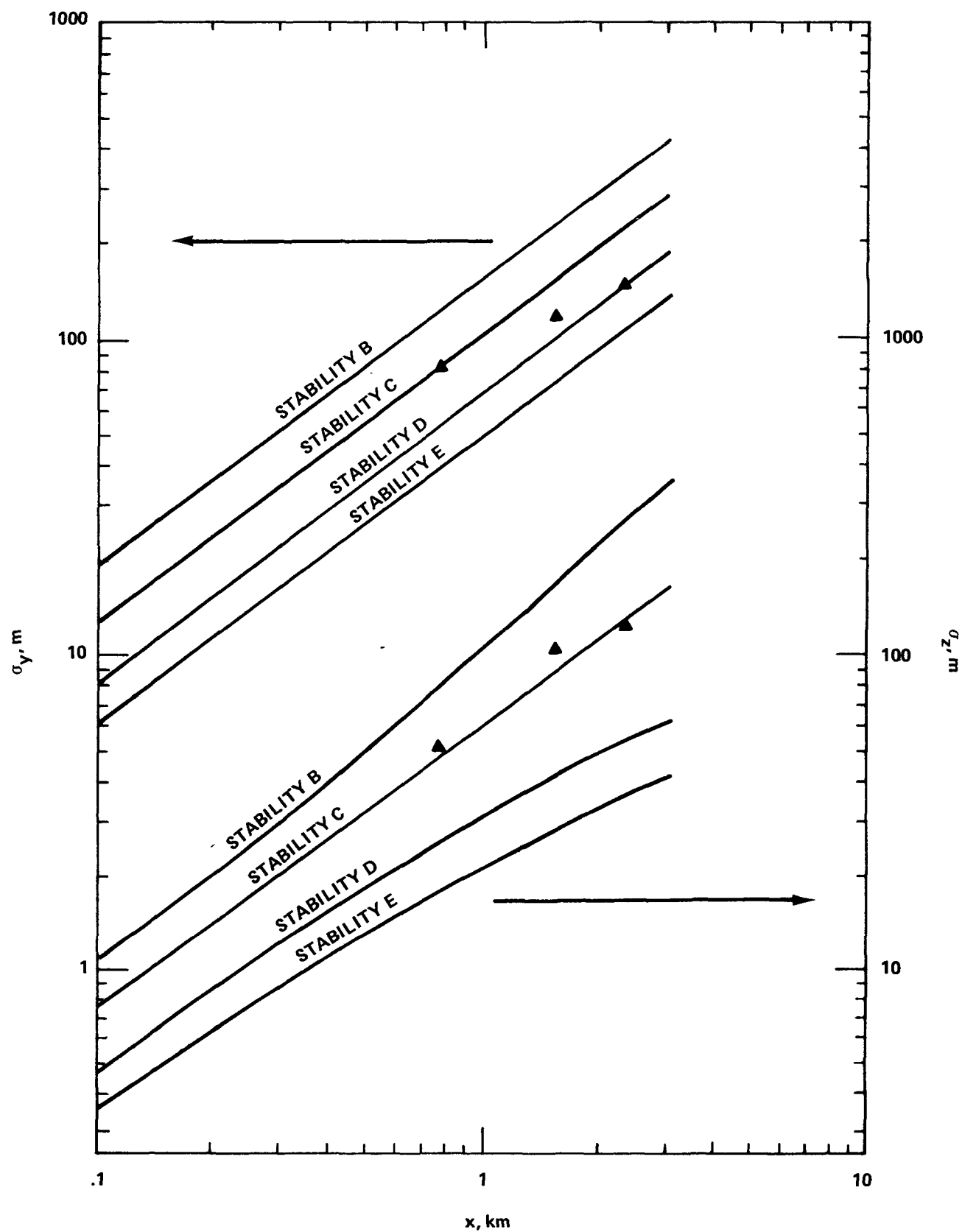


Figure 42. Estimated wind tunnel dispersion parameters compared with standard Pasquill-Gifford values (Turner, 1967).

TECHNICAL REPORT DATA		
(Please read Instructions on the reverse before completing)		
1. REPORT NO. EPA-600/4-79-051	2.	3. RECIPIENT'S ACCESSION NO.
4. TITLE AND SUBTITLE THE EPA METEOROLOGICAL WIND TUNNEL Its Design, Construction and Operating Characteristics	5. REPORT DATE September 1979	6. PERFORMING ORGANIZATION CODE
7. AUTHOR(S) W.H. Snyder	8. PERFORMING ORGANIZATION REPORT NO. Fluid Modeling Report No. 6	
9. PERFORMING ORGANIZATION NAME AND ADDRESS Environmental Sciences Research Laboratory Office of Research and Development U.S. Environmental Protection Agency Research Triangle Park, NC 27711	10. PROGRAM ELEMENT NO. 1AA603 AB-20 (FY-78)	11. CONTRACT/GRANT NO.
12. SPONSORING AGENCY NAME AND ADDRESS Environmental Sciences Research Laboratory - RTP, NC Office of Research and Development U.S. Environmental Protection Agency Research Triangle Park, NC 27711	13. TYPE OF REPORT AND PERIOD COVERED in-house 6/75 - 12/78	14. SPONSORING AGENCY CODE EPA/600/09
15. SUPPLEMENTARY NOTES		
16. ABSTRACT The design philosophy, construction details, and operating characteristics of the EPA Meteorological Wind Tunnel are described. Measurements in the empty tunnel show that the mean velocity is uniform to within $\pm 2\%$ at any given cross section, at speeds as low as 1.5 m/s. The turbulence intensity in the empty tunnel is typically 0.5%. A 2-meter-deep boundary layer was obtained using elliptic wedge vortex generators and roughness on the floor. Measurements are presented showing that this boundary layer simulates, in both turbulence structure and dispersive characteristics, a neutral atmosphere boundary layer over rural terrain.		
17. KEY WORDS AND DOCUMENT ANALYSIS		
a. DESCRIPTORS Air pollution * Wind (meteorology) * Wind tunnels * Atmospheric diffusion * Design	b. IDENTIFIERS/OPEN ENDED TERMS	c. COSATI Field/Group 13B 04B 04A 13M
18. DISTRIBUTION STATEMENT RELEASE TO PUBLIC	19. SECURITY CLASS (This Report) UNCLASSIFIED	21. NO. OF PAGES 78
	20. SECURITY CLASS (This page) UNCLASSIFIED	22. PRICE

United States
Environmental Protection
Agency

Environmental Research Information
Center
Cincinnati OH 45268

Official Business
Penalty for Private Use
\$300

Postage and
Fees Paid
Environmental
Protection
Agency
EPA-335



Please make all necessary changes on the above label,
detach or copy and return to the address in the upper
left-hand corner.

If you do not wish to receive these reports CHECK HERE ☐
detach or copy this cover, and return to the address in the
upper left hand corner

EPA-600/4-79-051